

On Isostasy at Atlantic-Type Continental Margins

G. D. KARNER¹ AND A. B. WATTS

*Lamont-Doherty Geological Observatory and Department of Geological Sciences of Columbia University
Palisades, New York 10964*

Cross-spectral techniques have been used to analyze the relationship between free air gravity anomalies and topography of approximately 100 profiles over the continental margins of eastern North America, southwest Africa, and the Coral Sea/Lord Howe Rise. The resulting admittance functions for these margins have been interpreted in terms of the flexure model of isostasy. The relatively young Coral Sea/Lord Howe rise margin is associated with the lowest value of the effective elastic thickness ($T_e < 5$ km), while the relatively old eastern North American margin is associated with the highest value ($10 < T_e < 20$ km). Thus T_e appears to increase with the age of the margin. These results, which are consistent with flexure studies from the major ocean basins, have been interpreted in terms of a simple model in which the flexural strength of the lithosphere increases with age. The model suggests that a low-rigidity plate (or Airy-type model) is most applicable early in rifting history, while a high-rigidity plate is more applicable later in margin evolution. Thus sediments at a margin initially load a relatively thin and hot plate, while sediments later in margin evolution load a relatively thick and cold plate. The model explains a number of features of the tectonic-stratigraphic evolution of margins. These include a change in flexural style from a narrow and deep basin to a broad and shallow basin, coastal plain onlap, and uplift in the continental interior. Furthermore, the flexure model of isostasy contributes in a major way to observed free air gravity anomalies at continental margins. In particular the model explains the existence of (Airy) isostatic gravity anomalies at margins. The amplitude and wavelength of these anomalies are a function of the sediment supply, the type of mechanisms controlling sediment deposition (up building and/or out building), and the thermal structure, history, and age of the margin.

INTRODUCTION

The concept of isostasy describes the manner in which topographic features on the earth's surface are compensated at depth. The two most commonly used models were those developed by Airy [1855] and Pratt [1855]. In the Airy model the crust is of constant density but is thicker beneath mountain ranges than lowlands. For the Pratt model the average crustal density is smaller beneath mountain ranges than lowlands. These models generally satisfied the early requirements of physical geodesy but initially were only of limited interest to geologists and geophysicists. Subsequent seismic studies showed that the Airy model, in particular, satisfactorily explained variations in crustal structure associated with such features as mountain ranges and continental margins [Heiskanen and Vening Meinesz, 1958; Worzel, 1965].

Worzel attributed the free air gravity anomaly at Atlantic-type continental margins to the transition between relatively thick continental crust and thin oceanic crust. This anomaly is generally characterized by a positive peak of up to +50 mgal over the outer continental shelf and a negative trough of up to -50 mgal over the continental slope and rise. Gray and Stacey [1970], Talwani and Eldholm [1972, 1973], and Rabinowitz [1974], for example, corrected the free air anomaly for crustal structure using the Airy model. They discussed the resulting isostatic gravity anomaly in terms of lateral density variations in the crust. In particular, Talwani and Eldholm [1972] interpreted the anomaly in terms of the ocean/continent boundary.

The Airy model, however, implies a crust that cannot support vertical shear stresses or their equivalent gravity

anomalies. J. Barrell argued as early as 1914 that isostatic equilibrium in the form envisaged by Airy could not exist everywhere on the earth's surface because of the finite strength of the crust. Barrell [1914] defined this strong rigid upper layer of the earth as the lithosphere.

A number of studies [Vening Meinesz, 1941; Walcott, 1970; Watts and Cochran, 1974; McNutt and Menard, 1978; Watts, 1978; Watts et al., 1980] have subsequently investigated the response of the lithosphere to surface loads such as seamounts and oceanic islands. These studies indicate that in a number of cases the response of the lithosphere to surface loads can be modelled as that of a thin elastic plate overlying a weak fluid. This model of isostasy, referred to as the flexure model, is similar to the Airy model in which surface loads are supported by crustal thickening, but differs by including the lateral strength of the crust. A useful parameter in the flexure model, which characterizes the response of the lithosphere to these loads, is the effective flexural rigidity. These studies show that the effective flexural rigidity of oceanic lithosphere ranges from 7×10^{26} to 1×10^{31} dyn-cm and is a strong function of crustal age and temperature.

The sediments which accumulate at a continental margin also constitute a load on the lithosphere. Gunn [1944], Walcott [1972], and Cochran [1973] showed that the character of the gravity anomalies and the sedimentary thicknesses at a continental margin are consistent with the flexure model. However, Walcott, by assuming a relatively high uniform effective flexural rigidity (2×10^{30} dyn-cm), was not able to explain the existence of relatively narrow ($\lesssim 150$ km) continental shelves.

Seismic reflection profiling has shown that continental margins are generally characterized by substantial thicknesses of seaward-dipping sediments overlying a faulted continental basement [Given, 1977; Austin et al., 1980; de Charpal et al., 1978]. Biostratigraphic studies show that

¹ Also at the Bureau of Mineral Resources, Canberra City, 2601, Australia.

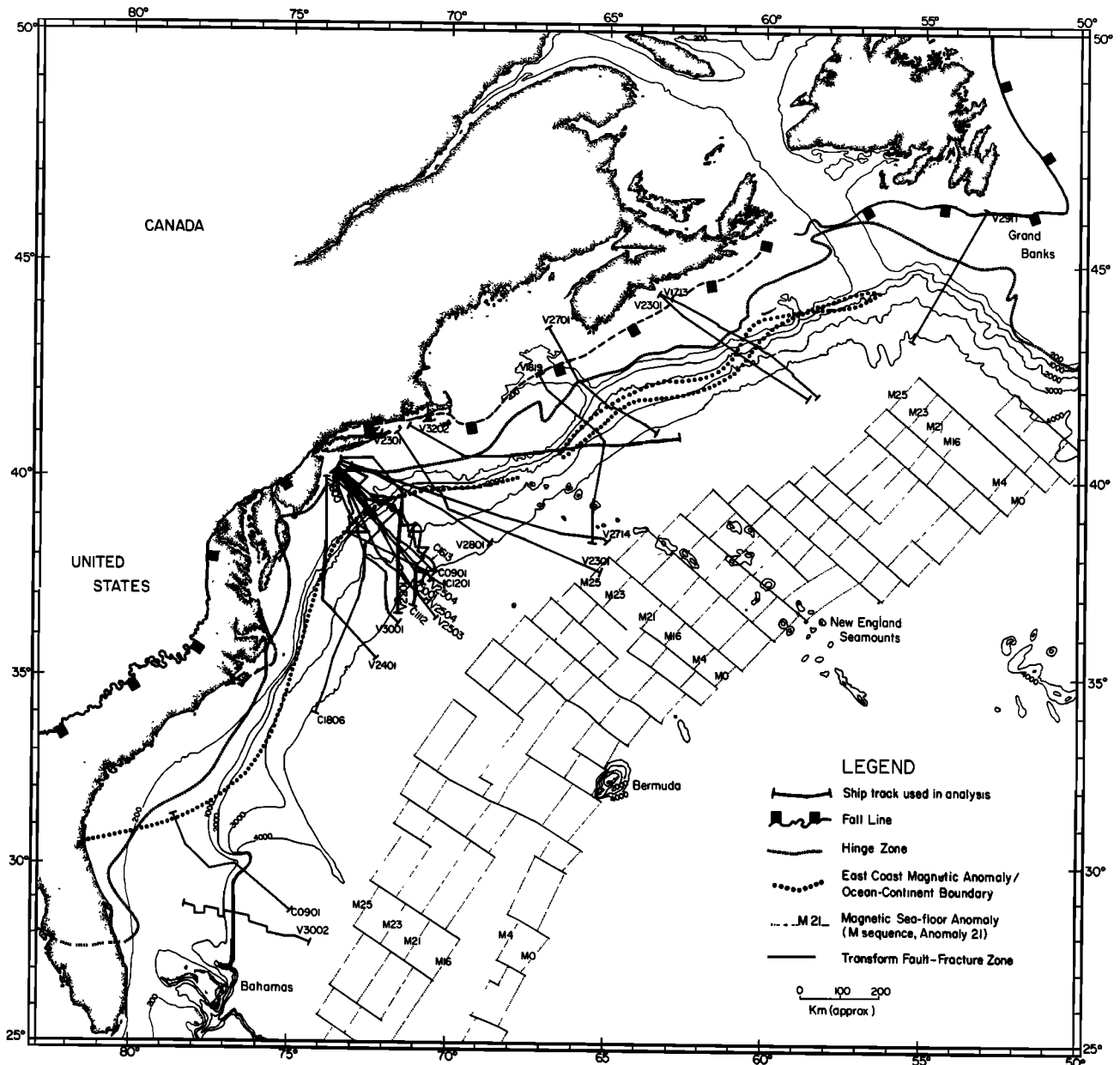


Fig. 1a. Location of free air gravity anomaly and topography profiles off eastern North America used in this study. The position of the land fall line is based on King [1969], Jansa and Wade [1975], and Austin *et al.* [1980] offshore. The southern location of the East Coast magnetic anomaly is from Rabinowitz [1974] and has been interpreted as representing the ocean-continent boundary [Folger *et al.*, 1979]. The North Atlantic Mesozoic magnetic anomaly sequence is from Schouten and Klitgord [1977]. The position of the hinge zone is based on Maher and Applin [1971], Jansa and Wade [1975], Dillon *et al.* [1979], and Austin *et al.* [1980]. Bathymetry (meters) is from Uchupi [1971].

most of these sediments were deposited in continental or shallow water marine environments. A number of studies [Sleep, 1971; Watts and Ryan, 1976; Steckler and Watts, 1978] have shown that the postrift tectonic subsidence of margins can be explained in terms of simple thermal cooling models. These observations suggest that the effective flexural rigidity, and therefore the state of isostasy, may vary during the evolution of the margin.

The overall objective of this paper is to determine information on the isostatic mechanism at Atlantic-type continental margins. In particular, we will determine whether the flexure model of isostasy, which has successfully been used at other geological features in oceans, is applicable at margins. The procedures we use are (1) to determine the relationship

between observed free air gravity anomalies and topography at margins, (2) to interpret this relationship in terms of different models of crustal as well as thermal isostasy, and (3) to use the preferred models of isostasy to better understand the origin and evolution of continental margins.

GEOLOGICAL SETTING

We have used in this study free air gravity anomaly and topography data from three Atlantic-type continental margins which differ in their age of formation and sedimentation history. The eastern North American margin has an age of ~170 m.y. b.p. with sediment thicknesses of 10–15 km; southwest Africa has an age of ~110 m.y. b.p. with 5–8 km of sediment primarily in the Orange River Basin; and the

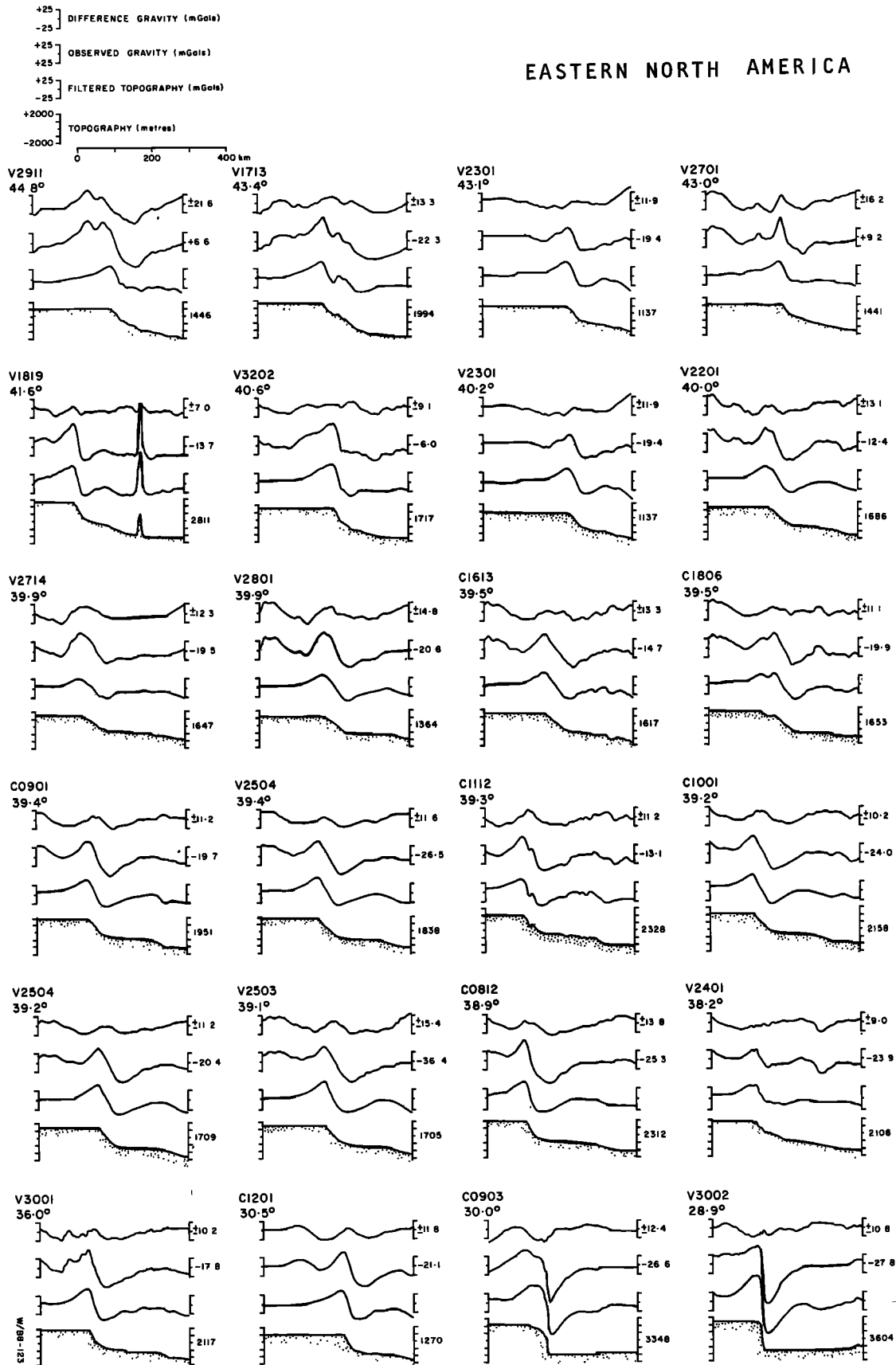


Fig. 1b. Data plot of observed free air gravity and bathymetry profiles of the tracks shown in figure 1a. Displayed also is the filtered topography (using the calculated eastern North American admittance function) or predicted free air gravity anomaly and the 'isostatic' gravity anomaly calculated as the difference between the observed and predicted free air gravity anomalies.

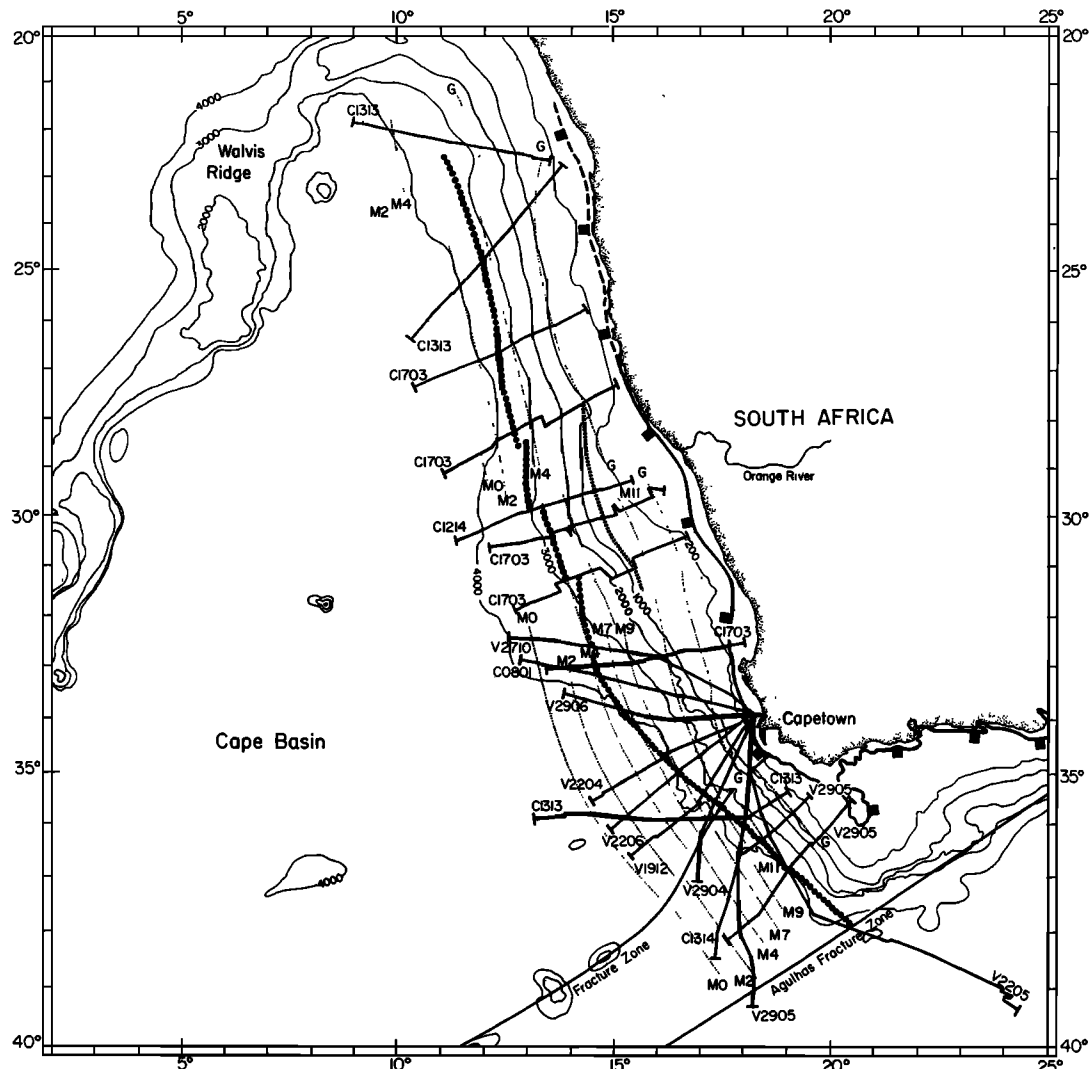


Fig. 2a. Location of free air gravity anomaly and topography profiles over the southwest African margin used in this study (the legend is as for Figure 1a). The position of the fall line is based on Dingle [1973]. The ocean-continent boundary can be defined by two conflicting criteria: (1) position of G magnetic anomaly [Rabinowitz, 1976] and (2) (preferred) transition from rough to smooth reflection seismic character of the basement [Gerrard and Smith, 1982]. The Cape Sequence magnetic spreading anomalies are from Rabinowitz [1976]. Hinge zone position is from Gerrard and Smith [1982] and is only known in the Orange River basin. Bathymetry (meters) is from Uchupi [1971].

Coral Sea/Lord Howe rise has an age of ~60 m.y. B.P. and sediment thickness generally less than 1 km. These margins therefore are suitable for the study of the state of isostasy at margins and how this varies with time.

The eastern North American margin (Figure 1) is characterized by substantial thicknesses (>10 km) of mainly shallow water Cenozoic and Mesozoic sediments. Rift sediments, primarily terrigenous clastics, volcanics, and evaporites were deposited in grabens formed by rifting of the basement rocks during the Late Triassic–Early Jurassic [Austin *et al.*, 1980]. These rift sediments crop out in the Newark and Connecticut basins and probably underlie the Cenozoic and Mesozoic sediments of the margin.

The margin is located adjacent to a magnetic quiet zone and magnetic anomaly M-25 (146 m.y. B.P., Van Hinte, [1976]). The age of basaltic volcanism associated with the formation of the margin is at the Lias/Trias boundary (195 m.y. B.P., Van Houten [1977]). These considerations therefore suggest an age for the formation of this margin at about 170 m.y. B.P.

Figure 1 summarizes the main structural elements of the eastern North American margin. The fall line represents the commencement of the gently dipping coastal plain sediments which gradually increase in thickness towards the hinge zone [Jansa and Wade, 1975; Watts and Steckler, 1979; Austin *et al.*, 1980]. The hinge zone is a major thermal and mechanical boundary at the margin and probably represents the transition between relatively unstretched continental crust and crust that has been stretched and thinned during rifting [Watts and Steckler, 1979]. The East Coast magnetic anomaly has been interpreted as indicating the location of the ocean-continent boundary [Rabinowitz, 1976; Folger *et al.*, 1979].

The South African margin consists of both rift and shear components. South of the Agulhas fracture zone, the margin is dominated by strike-slip faulting and exhibits truncated continental structures. The margin north of the fracture zone (used in this analysis) varies considerably in width and sediment thickness.

Figure 2 summarizes the main structural elements for the

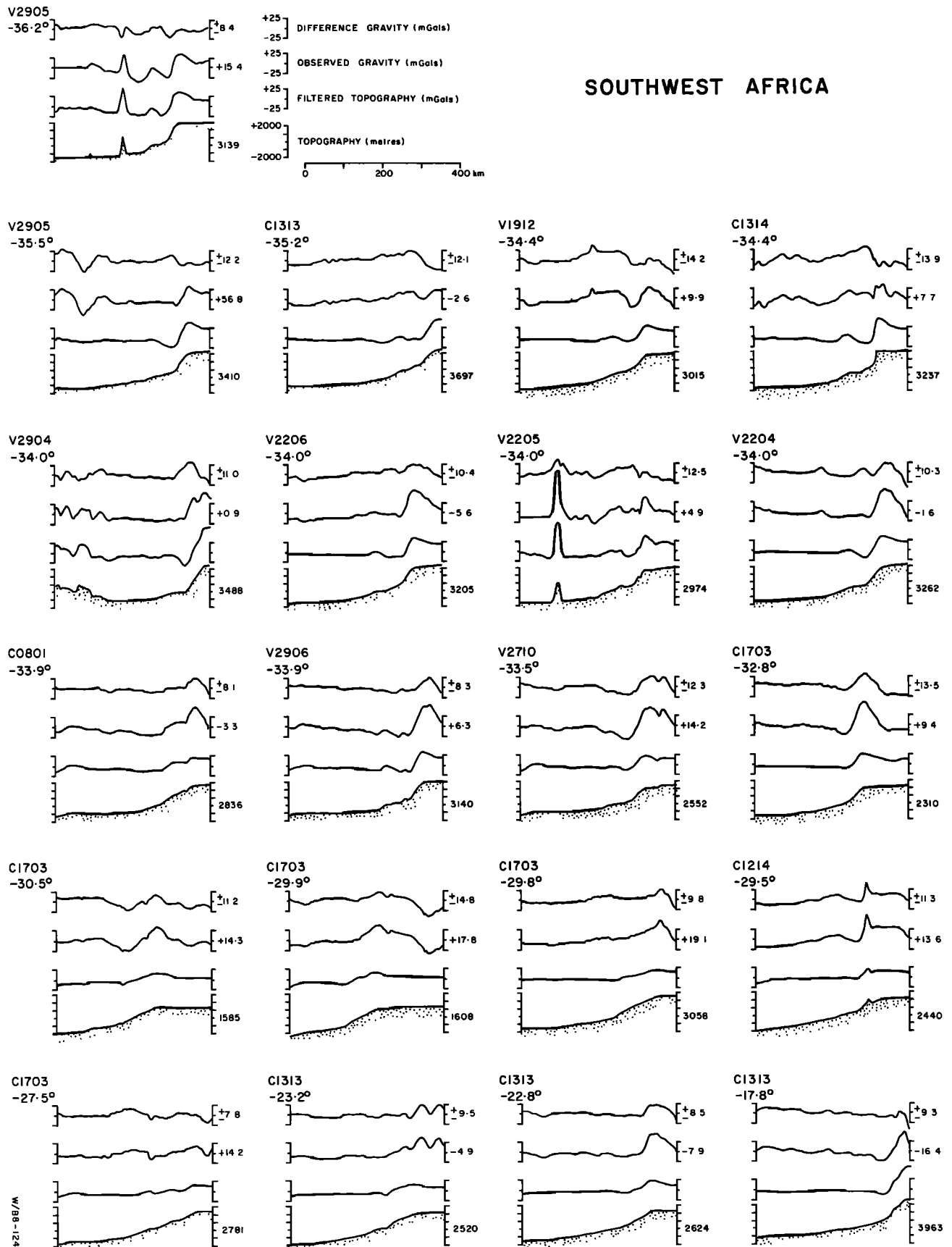


Fig. 2b. Data plot of observed free-air gravity and bathymetry profiles of the tracks shown in Figure 2a. Format is identical to Figure 1b.

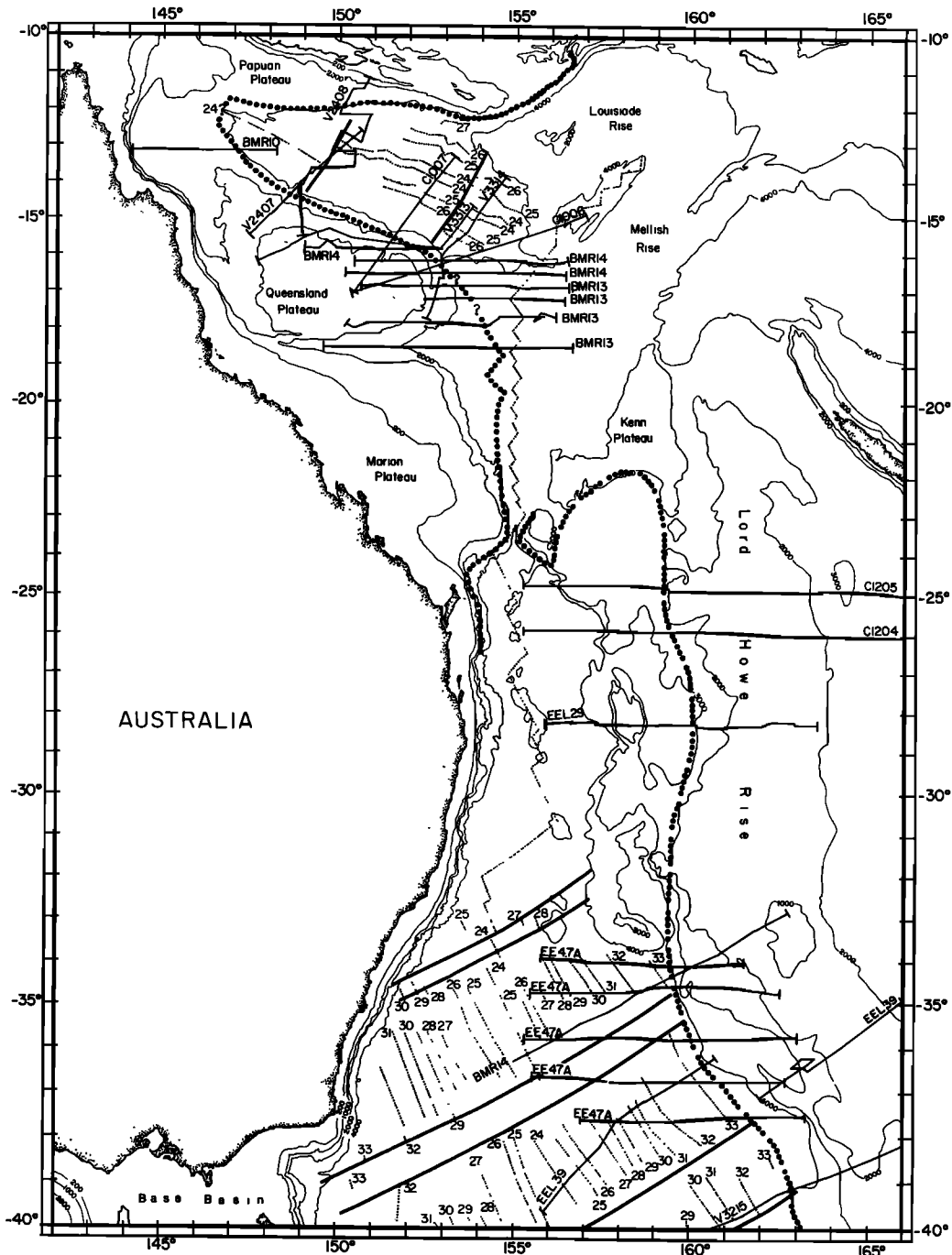


Fig. 3a. Location of free air gravity anomaly and topography profiles over the Queensland Plateau and Lord Howe rise used in this study (the legend is as for Figure 1a). The location of the ocean-continent boundary around the Coral Sea is from Mutter and Karner [1980] and Taylor and Falvey [1977]. The Tasman Sea ocean-continent boundary is based on reflection seismic and magnetic data. The magnetic spreading anomalies from the Coral and Tasman Seas are from Weissel and Watts [1979] and Weissel and Hayes [1977], respectively. Bathymetry (meters) has been modified from Mammerickx et al. [1974].

South African margin. Mesozoic magnetic lineations M0-M11 (the Cape Sequence) indicate the oldest oceanic crust is 128 m.y. B.P. [Rabinowitz, 1976; Larson and Ladd, 1973] thereby dating the age of the margin. This age has been substantiated by DSDP sites 360 and 361 [Shipboard Scientific Party, 1978]. The identification of the Mesozoic magnetic anomalies in the Orange River Basin is, however, in doubt. The G anomaly (Figure 2) has been interpreted as representing the ocean-continent boundary [Rabinowitz and LaBrecque, 1979]. Commercial drilling seaward of the G

anomaly, however, terminated in acidic lavas, volcanoclastics, and intercalated basalts and redbeds, which are interpreted as overlying continental basement [Gerrard and Smith, 1982]. We show in Figure 2 the most likely location of the ocean-continent boundary based on seismic data [Gerrard and Smith, 1982].

The stratigraphy and nature of the earliest rift sediments for this margin are, however, poorly known. Seismic refraction data [Rabinowitz, 1976] indicate that a large portion of the margin formed by progradation of the sediments. Prelim-

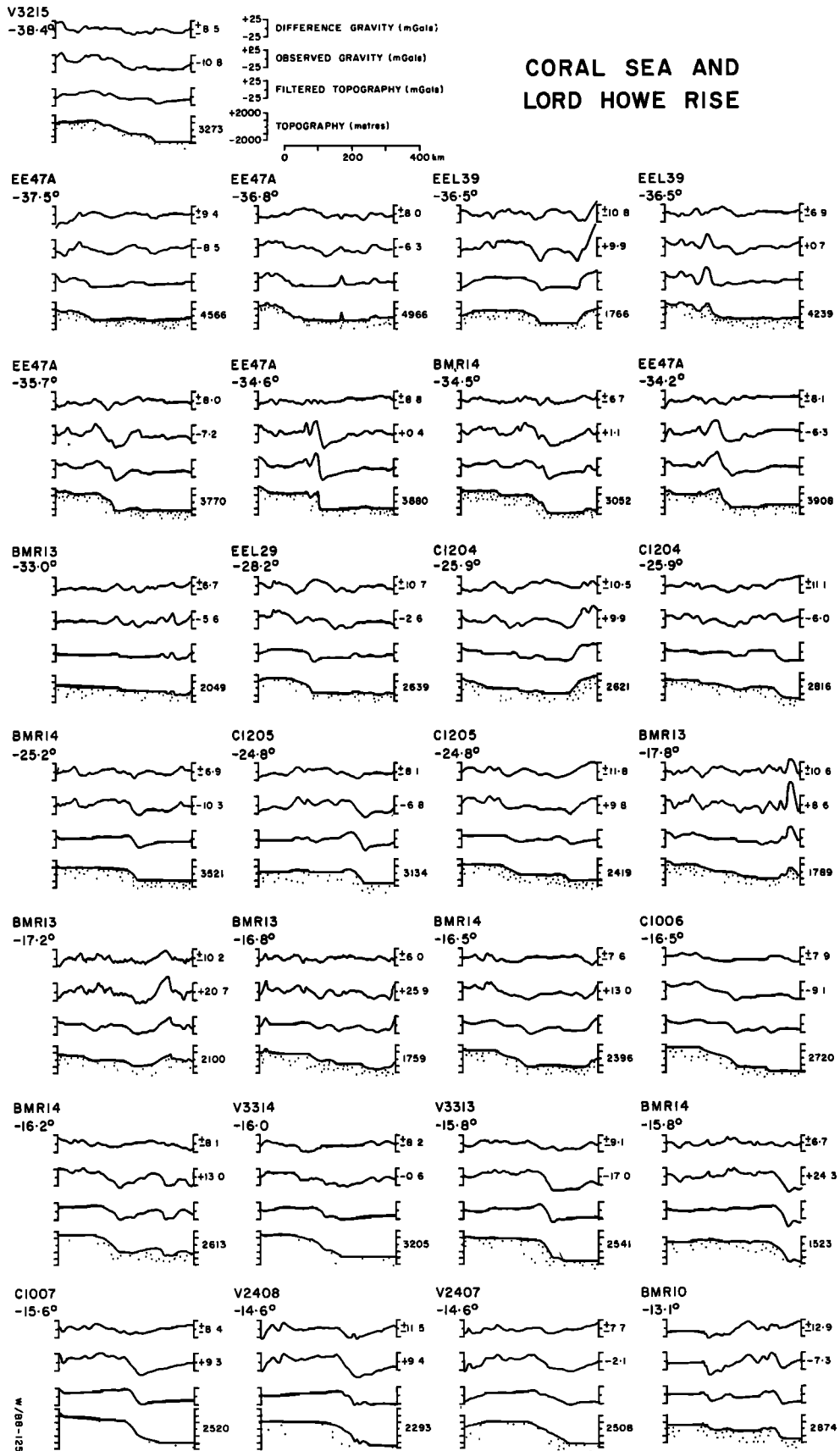


Fig. 3b. Data plot of observed free air gravity and topography profiles of the tracks shown in Figure 3a. The format for observed, predicted, and 'difference' gravity is as for Figure 1b.

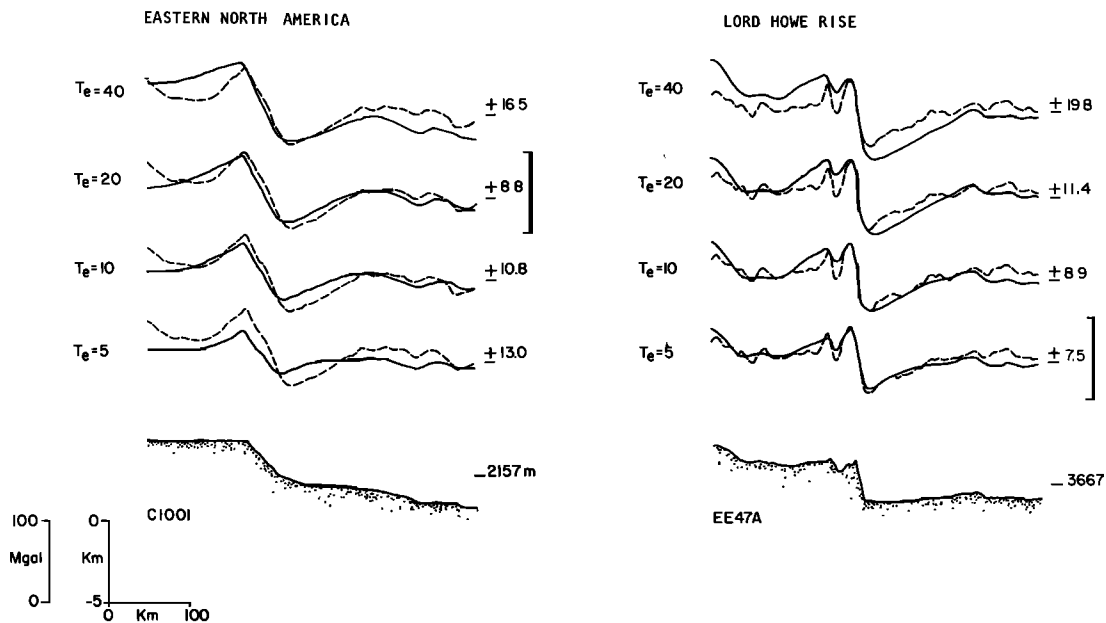


Fig. 4. Comparisons of observed free air gravity anomaly profiles (dashed line) with computed profiles (solid line) based on the flexure model for a range of T_e , the effective elastic thickness. T_e ranging from low to high values characterizes on and off ridge type loading, respectively. For the eastern North American margin the best fitting T_e , in a least squares sense, is for $T_e \sim 20$ km, while for the Lord Howe rise, $T_e \sim 5$ km. The ship cruise identification, mean topographic depths, and RMS values for each value of T_e are displayed on the respective topographic profiles.

inary commercial drilling indicates the margin is comprised of a sequence of Cretaceous to Cenozoic sediments which overstep pre-Mesozoic basement rocks [Gerrard and Smith, 1982].

The eastern Australian margin (Figure 3) is generally characterized by an absence of postrift sediments. Isolated rift grabens associated with the opening of the Coral and Tasman seas exist west of the Queensland Plateau and in the Bass Basin (Figure 3). Numerous narrow rift grabens appear to underlie the western margin of the Lord Howe Rise [Willcox *et al.*, 1980].

Geological and geophysical data suggest that the Queensland Plateau and Lord Howe Rise are underlain by continental basement [Mutter and Karner, 1980; Willcox *et al.*, 1980]. These margins are adjacent to magnetic anomalies 24 to 33 in the Coral Sea and Tasman Sea basins [Weissel and Hayes, 1977; Weissel and Watts, 1979], suggesting the age of formation of these margins is about 60 and 75 m.y. B.P., respectively.

We show typical free air gravity anomaly and topography profiles of the eastern North American and Coral Sea/Lord Howe rise margins in Figure 4. The relatively old eastern North American margin is characterized by large-amplitude gravity anomalies (peak to peak, 100 mgal) and a dominant wavelength of 150–200 km. In comparison the relatively young Coral Sea/Lord Howe rise margin is characterized by small-amplitude gravity anomalies (peak to peak, 60 mgal) and longer wavelengths (up to 400 km). The topography of this margin is generally similar, showing a well-developed shelf, slope, and rise.

We have investigated, in a preliminary way, the state of isostasy at these margins in Figure 4. For the case of the Coral Sea/Lord Howe rise margin, where there are only small sediment thicknesses, the state of isostasy will reflect the crustal structure of the margin produced at the time of rifting. The loading effects associated with thick sediment

accumulations, such as at the eastern North American margin, will, however, modify the state of isostasy by changing the crustal structure. Studies of the response of oceanic lithosphere due to surface loads, such as seamounts and oceanic islands, suggest the flexural strength of the lithosphere is a strong function of temperature [Watts, 1978; Watts *et al.*, 1980]. Sleep [1971], Watts and Ryan [1976], and Steckler and Watts [1978] have shown that the subsidence of margins not related to sediment loading is caused by thermal contraction due to cooling and thickening of the lithosphere. We would expect, therefore, that sediment loads formed on a young lithosphere should be associated with small values of the flexural rigidity, while loads formed on old lithosphere should be associated with higher values.

Figure 4 compares selected observed free air gravity anomaly profiles of the eastern North American and Coral Sea/Lord Howe margins with calculated profiles based on a simple plate model in which the flexural rigidity of the plate varies only as a function of time. The calculated profiles are based on a range of assumed flexural rigidity from 1×10^{28} dyn-cm (corresponding to an effective elastic thickness, $T_e = 5$ km) to 5×10^{30} dyn-cm ($T_e = 40$ km) which corresponds to loading on young and old lithosphere, respectively [Watts *et al.*, 1980, Figure 1]. This figure shows that the selected profile for the eastern North American margin can be most satisfactorily explained by a relatively high effective elastic thickness ($T_e \sim 20$ km), while the profile for the Coral Sea/Lord Howe rise margin can be explained by a low effective elastic thickness ($T_e \sim 5$ km). We investigate these apparent differences in the state of isostasy at margins quantitatively in the following sections.

CRUSTAL ISOSTASY

Previous interpretations of free air gravity anomalies at continental margins have been in terms of isostatic models which only considered variations in crustal structure. There

are two main types of crustal isostatic models: one in which compensation is achieved by lateral density variations (for example, Pratt-Hayford models) and the other in which compensation results from changes in crustal thickness (for example, Airy and flexure models). The two most commonly used models at margins have been the Airy and flexure models [Worzel, 1965; Talwani and Eldholm, 1972, 1973; Walcott, 1972; Cochran, 1973; Rabinowitz, 1974; Sobczak, 1975].

Isostatic Models

A useful method of quantitatively determining the state of isostasy at a geological feature was developed by Dorman and Lewis [1970]. This method assumes that free air gravity anomalies are caused by topography and its compensation, and attempts to determine a function which, when convolved with topography, reproduces the gravity anomaly. The advantage of this method is that this function may be derived from observational data, independent of a particular isostatic model. Once the function has been determined, however, it can be interpreted in terms of simple models of isostasy.

By the repeated use of Green's equivalent layer theorem, it is possible to construct theoretical admittance functions which represent isostatic processes. The Fourier or frequency domain gravity effect of a topographic surface, $h(x)$, at a depth d from the measuring plane and of density ρ , is given by (for $d \gg h(x)$),

$$G(k) = 2\pi\gamma\rho e^{-kd}H(k) \quad (1)$$

where k , the wavenumber, is related to wavelength λ by $k = 2\pi/\lambda$, γ is the gravitational constant, and the uppercase symbols refer to the Fourier transform of the corresponding functions designated by lowercase symbols.

For simplicity it is usually assumed that compensation is totally achieved at a single interface and that the depth to this interface, the depth of compensation, T_c , is the crustal thickness. Because of isostatic compensation, the resultant gravity effect of the surface topography will result from the destructive interference of the gravity effects of the surface and the compensating interface. By (1) the gravity effect of the surface topography (in the Fourier domain) is

$$G_1(k) = 2\pi\gamma\Delta\rho_1 e^{-kd}H(k) \quad (2)$$

where $\Delta\rho_1$ is the density contrast across the surface topography, d is the mean elevation, and $H(k)$ the Fourier transform of the surface topography $h(x)$. The gravity effect of the root topography is

$$G_2(k) = -2\pi\gamma\Delta\rho_2 e^{-k(d+t)}R(k) \quad (3)$$

where $\Delta\rho_2$ is the density contrast across the root topography, t is the distance between the mean surface and root topography, and $R(k)$ the Fourier transform of the root topography $r(x)$. The general equation for the gravity effect of a two-layer isostatic model is therefore

$$G_T(k) = 2\pi\gamma\Delta\rho_1 H(k) e^{-kd} \left[1 - \frac{\Delta\rho_2 R(k)}{\Delta\rho_1 H(k)} e^{-kt} \right] \quad (4)$$

The rheology of the lithosphere determines the process by which compensation is achieved, which, with the density contrasts across the interfaces involved in the compensa-

tion, determines the relation between $r(x)$ and $h(x)$. If we assume an elastic rheology for the lithosphere, then the relation between $R(k)$ and $H(k)$ can be expressed as [Banks *et al.*, 1977]

$$R(k) = \frac{\Delta\rho_1}{\Delta\rho_3} \left[1 + \frac{k^4 D}{\Delta\rho_3 g} \right]^{-1} H(k) \quad (5)$$

where D is the effective flexural rigidity and $\Delta\rho_3$ is the density contrast between the material underlying the plate and the material infilling the flexural basin. As $D \rightarrow 0$, $R(k) \rightarrow (\Delta\rho_1/\Delta\rho_3) H(k)$, which corresponds to sediment loading on a very weak plate and is termed 'Airy loading.' However, as the density of the material infilling the basin approaches the crustal density, $R(k) \rightarrow (\Delta\rho_1/\Delta\rho_2) H(k)$, which is the familiar Airy model. The flexure model therefore lends itself as a first-order mechanical model for the study of isostasy. In particular, uncompensated, regional, and Airy isostatic schemes may be represented by the flexural response of the lithosphere for rigidities which range from high to low values.

The theoretical admittance $Z(k)$ can be determined for both the Airy and flexure models of isostasy by substituting various forms of (5) into (4). For example, as $D \rightarrow 0$ and $\Delta\rho_3 \rightarrow \Delta\rho_2$, (4) becomes

$$G_A(k) = 2\pi\gamma\Delta\rho_1 H(k) e^{-kd} [1 - e^{-kt}] \quad (6)$$

and normalizing by the transform of the surface topography $H(k)$ gives the Airy admittance,

$$Z_A(k) = 2\pi\gamma\Delta\rho_1 e^{-kd} [1 - e^{-kt}] \quad (7)$$

Similarly, the flexure admittance is obtained by substituting (5) into (4) and normalizing by $H(k)$ so that

$$Z_p(k) = 2\pi\gamma\Delta\rho_1 e^{-kd} \left\{ 1 - \frac{\Delta\rho_2}{\Delta\rho_3} \left[1 + \frac{k^4 D}{\Delta\rho_3 g} \right]^{-1} e^{-kt} \right\} \quad (8)$$

Figure 5 shows computed free air gravity anomaly profiles for the Airy and flexure models of isostasy at a continental margin. The upper model represents the case of a sediment-starved margin while the middle and lower models represent the loading of the margin by sediments. The middle model is for $D = 0$ and the lower model is for $D = 9 \times 10^{28}$ dyn-cm ($T_e = 10$ km). The calculated profiles are based on the Fourier method (solid lines) and the line-integral method (dots) [e.g., Talwani, 1973]. The methods are in general agreement for the upper model. The main differences occur over the inflection points in the topography and are caused by errors introduced by using the approximation in (1). The methods are not in as good agreement, however, for the middle and lower models because these models include density differences within the crust; in particular, the existence of a hinge zone. These density differences are not related to the topography and therefore cannot be predicted using the Fourier method. The largest differences in the computed gravity anomalies occur at the hinge zone and decrease with increasing flexural rigidity. Figure 5 shows that the energy in the computed gravity anomaly is divided between the hinge zone and the shelf edge and the amplitude and wavelength of the gravity anomaly is controlled by the sediment distribution and the rigidity of the plate.

The main result from Figure 5 is that the Fourier method successfully predicts the free air gravity anomaly over a

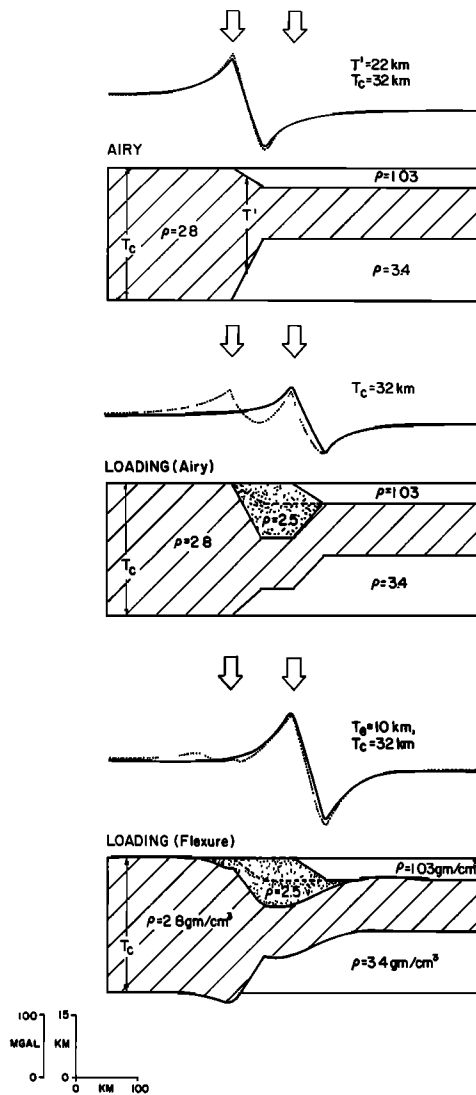


Fig. 5. Theoretical loading of a passive margin, initially in Airy compensation, by a sediment wedge. Each model compares the gravity effect calculated by the line integral method (dotted line) and the Fourier method (solid line). 'Airy loading' results when sediments load a margin which has an effective elastic thickness of zero, whereas 'Airy' essentially refers to the crustal structure of a sediment starved margin (T' refers to the apparent crustal thickness, for which the expression is given in Figure 6a). 'Flexural loading' results when sediments load a margin with an effective elastic thickness greater than zero; in this case, $T_e = 10$ km. The gravity effect calculated using the Fourier method is in good agreement with the line-integral technique for the Airy (classical) and Loading (flexure) models. The Fourier method cannot, however, predict the double-peaked anomaly of the loading (Airy) model because the hinge zone has no topographic expression. Note the progressive shift in the free air gravity 'edge effect' anomaly as mass is transferred across the margin. Initially, the energy in the gravity anomaly is shared between the hinge zone and the shelf break. As the rigidity increases, the energy is transferred from the hinge zone to the shelf break anomaly.

continental margin. In particular the large differences in water depths along the profile, the position of the ocean-continent boundary, the changes in crustal thickness, and the hinge zone have a small overall effect on the calculated gravity anomaly.

We have used in Figure 5 a 'classical' Airy model in which the crustal density is constant ($\rho = 2.8$ gm/cm³). The

isostatic model introduced by *Talwani and Eldholm* [1972], though having the fundamental form of an Airy-type model, was based on varying crustal density contrasts of -1.57 gm/cm³ and 0.47 gm/cm³ at the water-crust and crust-mantle interfaces, respectively. A water density of 1.03 gm/cm³, however, implies an unreasonable mantle density of 3.07 gm/cm³. The classical Airy model of Figure 5 therefore differs from the model used by *Talwani and Eldholm* [1972], *Rabinowitz* [1974], and *König and Talwani* [1977] in that a horizontal layer of zero-density contrast separates the surface topography from the root topography and is appropriately termed the 'hidden layer' Airy model. However, since the gravity effects of the classical Airy model for $\rho = 2.5$ gm/cm³ and 2.8 gm/cm³ and the hidden layer Airy model with the above density contrasts differ by less than 5 mgals, these models can be used interchangeably.

Theory

We presented in the previous section the formulation of theoretical admittance functions for the Airy and flexure models. In this section the theory for the determination of an admittance function from observed free air gravity and topography data at a continental margin is presented. The observed admittance functions can then be used to infer the state of isostasy at a margin by comparison with theoretical functions.

The admittance function contains information about the in-phase components of both gravity and topography. The gravity anomaly $\Delta g(x)$, associated with a two-dimensional topographic feature, can be written in the form

$$\Delta g(x) = \int_{-\infty}^{+\infty} H(\eta)K(\rho, d, x - \eta) d\eta \quad (9)$$

where $K(x, \rho, d)$ is a kernel dependent on the surface or topographic density ρ , the mean topographic height d , and the distance from the topographic feature, x [Bott, 1973]. Equivalently, this can be written

$$\Delta g(x) = h(x) * K(x, \rho, d) \quad (10)$$

where $*$ represents the convolution of $h(x)$ with the kernel $K(x, \rho, d)$. In the frequency domain, convolution becomes a simple product. Rewriting the above equation in the frequency domain,

$$F[\Delta g(x)] = F[h(x)]F[K(x, \rho, d)] \quad (11)$$

therefore

$$K(x, \rho, d) = F^{-1}[F[\Delta g(x)]/F[h(x)]] \quad (12)$$

where $F[]$ represents the Fourier transform of the spatial data series $h(x)$ and $g(x)$ and $F^{-1}[]$ represents the inverse transform. In particular, $F[K(x, \rho, d)]$ is the admittance function and $K(x, \rho, d)$ is the equivalent spatial transfer filter. A full description of this technique has been given by *Lewis and Dorman* [1970], *McKenzie and Bowin* [1976], and *Watts* [1978].

The topography of a continental margin can be represented as a signum function convolved with a narrow rectangular gate (see the appendix). By reflecting $h(x)$ and $g(x)$, the transforms become real and stable while the admittance remains invariant to this reflection. Geologically, the reflected $h(x)$ would be interpreted as a wide plateau.

The gravity and topography data have been prepared in

this study by linearly interpolating, reflecting, and then sampling using a rectangular window. All data has been projected normal to the local trend of the margin, the shelf break being approximately in the center of each profile where possible. To obtain stable spectral estimates of a single geological feature, in this case the margin, spectral smoothing is accomplished by using a number of profiles of 400-km length, each of which statistically represents an independent estimate of the admittance.

The result of this analysis is an observed admittance function which reproduces the gravity over a margin from the topography and is not tied to a particular isostatic model. The admittance function reliably represents the margin studied if the ratio of the observed to predicted energy of the gravity anomalies is high.

Results

By applying the admittance function approach to the analysis of free air gravity anomaly and topography profiles (appendix), it is possible to investigate the isostatic mechanism operative at Atlantic-type continental margins. The interpretation of the observed admittance function in terms of an isostatic model involves assumptions concerning the rheology and density structure of the margin.

Figure 6 shows the observed admittance function determined from 24 free air gravity anomaly and topography profiles of the eastern North American margin (Figure 1). For wavenumber $k = 0.040\text{--}0.180$ ($\lambda = 157\text{--}35$ km) the admittance gently decreases and is controlled mainly by the mean water depth along the margin. For $k = 0.015\text{--}0.040$ (419–157 km), however, the admittance rapidly increases due to the effects of isostasy. From (2) we have

$$\ln [Z(k)] = -kd + \ln [2\pi\gamma(\rho_2 - \rho_w)] \quad (13)$$

Estimates of ρ_2 and d can be determined from the slope and intercept of the observed admittance function (note that ρ_2 is the density which would be required for the Bouguer reduction) for $k > 0.04$ km⁻¹ (157 km). For the eastern North American margin, estimates of ρ_2 , the average density of topography, and d , the mean water depth, are 2.45 gm/cm³ and 3.0 km, respectively. The estimate of ρ_2 is in good agreement with well log data along the eastern North American margin.

In order to determine the isostatic parameters of the eastern North American margin, the calculated admittance function has been compared with theoretical Airy and flexure admittance functions (Figure 6). Theoretical admittance functions for the Airy model fit the observations for $k = 0.015\text{--}0.050$ (419–126 km). The best fit, in a least square sense, to the theoretical admittance is for $T_c = 40\text{--}110$ km and $T_e = 10\text{--}20$ km.

Figure 7 shows the observed admittance function determined from 21 free air gravity anomaly and topography profiles of the South African margin (Figure 2). Estimates of ρ_2 and d of 2.4 gm/cm³ and 3.25 km were obtained, respectively. Theoretical admittance functions for the Airy and flexure models for $k = 0.015\text{--}0.060$ (419–105 km) give estimates for this margin of $T_c = 28$ to 108 km and $T_e = 5\text{--}10$ km, respectively.

Figure 8 shows the observed admittance function determined from 29 free air gravity and topography profiles: 14 from the Coral Sea and 15 from the Lord Howe rise.

Estimates of ρ_2 and d of 2.40 gm/cm³ and 3.0 km were obtained, respectively. Theoretical admittance functions for the Airy model for $k = 0.015\text{--}0.180$ (419–35 km) give estimates for this margin of $T_c = 18\text{--}28$ km and $T_e < 5$ km.

By convolving the observed admittance functions with topography, an estimate of the free air gravity anomaly can be obtained for each margin profile. The close similarity between observed and predicted gravity anomalies (Figures 9, 1b, 2b, 3b) indicates the observed admittance functions in Figures 6–8 adequately represent the relationship between gravity and topography for the eastern North American, southwest African, and Coral Sea/Lord Howe rise margins, respectively. The differences between observed and predicted gravity anomalies are caused by density differences within the crust that are not common between profiles over the length of the margin. Since these differences are small, the observed admittance functions can be interpreted with some confidence in terms of different isostatic models.

We have interpreted the admittance functions for each margin in terms of the Airy and flexure models of isostasy. The Airy model can be considered as a special case of the plate model ((6), $D \rightarrow 0$, $\Delta\rho_3 \rightarrow \Delta\rho_2$). Thus by varying D in the flexure model we are considering the general scheme of isostasy rather than a specific end member. Furthermore, the flexure model has been successfully applied to a number of other oceanic geological features [Watts *et al.*, 1980]. The results in Figure 6–8 therefore indicate that the effective elastic thickness T_e of the lithosphere increases with age of the margin. The relatively old eastern North American margin is associated with the highest values of T_e while the relatively young Coral Sea/Lord Howe rise margin is associated with the lowest values. The values obtained for the margins ($T_e < 20$ km) are significantly smaller than values obtained from seamount and oceanic island loads in the plate interiors ($20 < T_e \leq 40$ km, Watts *et al.* [1980]) but are similar to values at or near midocean ridge crests ($1 < T_e < 10$ km, Cochran [1979] and McNutt [1979]). These results (Figures 6–8) from spectral analysis are therefore consistent with the earlier observation (Figure 4) that the free air gravity edge effect anomaly at a margin is predominately controlled by flexure of the lithosphere.

THERMAL ISOSTASY

So far we have assumed that the observed free air gravity anomaly is related only to the crustal structure of the continental margin. However, associated with the processes of rifting, the lithosphere is either heated or replaced by hotter, asthenospheric material. The changes in temperature produce a corresponding change in density determined by the coefficient of thermal expansion, α . As the temperature anomalies associated with rifting dissipate by vertical and horizontal conductive heat transfer, therefore, the gravity anomaly will change during the evolution of the margin. Since mass is conserved during the rifting process and subsequent margin development, the gravity anomaly at any one time will integrate to zero. We refer to this redistribution of mass during margin development as thermal isostasy.

The total gravity effect at an Atlantic-type continental margin will therefore be a result of superposing the gravity effects of crustal and thermal isostasy. In order to determine the thermal gravity effect, it is necessary to model the temperature variations at a margin caused by the initial

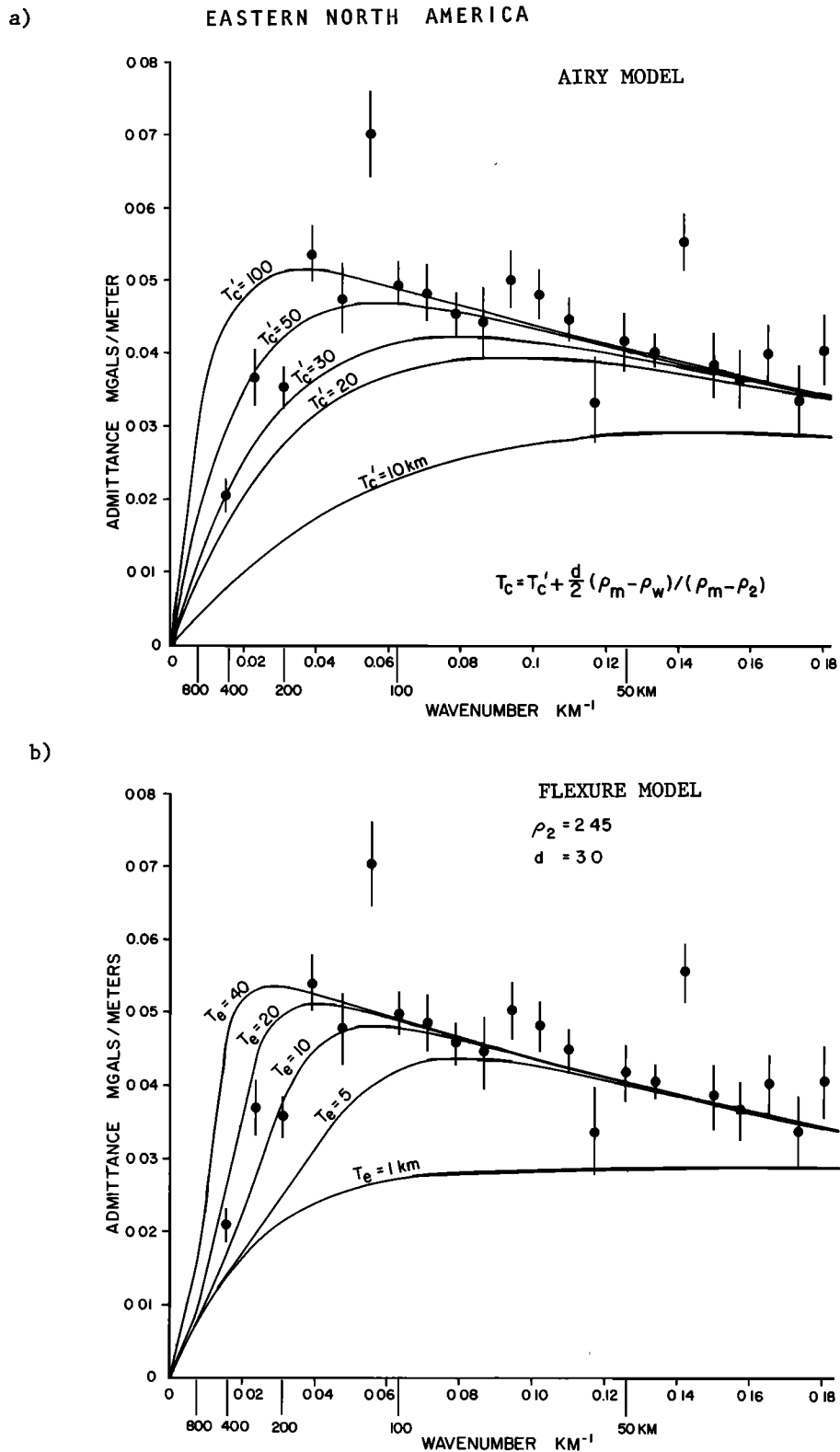


Fig. 6. (a) Observed admittance values (solid circles) estimated from free air gravity anomaly and topography profiles for the eastern North America margin. The standard deviation of each estimate is computed assuming a normal probability distribution for the ratio of true-sample admittance: $\sigma = [(\gamma^2 - 1)/2p]^{1/2}$, where p is the number of independent estimates of the admittance and γ^2 is the coherence or correlation coefficient between true and sample admittance. The solid curves indicate the theoretical admittance for the Airy model of isostasy for varying T_c' , the apparent crustal thickness. The theoretical models are constructed using the estimated parameters ρ_2 and d from the y intercept and slope of the observed admittance curve (Figure A3). (b) Observed admittance values (solid circles) for eastern North America, compared with theoretical admittance models based on the flexure model of isostasy for varying T_e , the effective elastic thickness. The estimated parameters used are the same as those in Figure 6a.

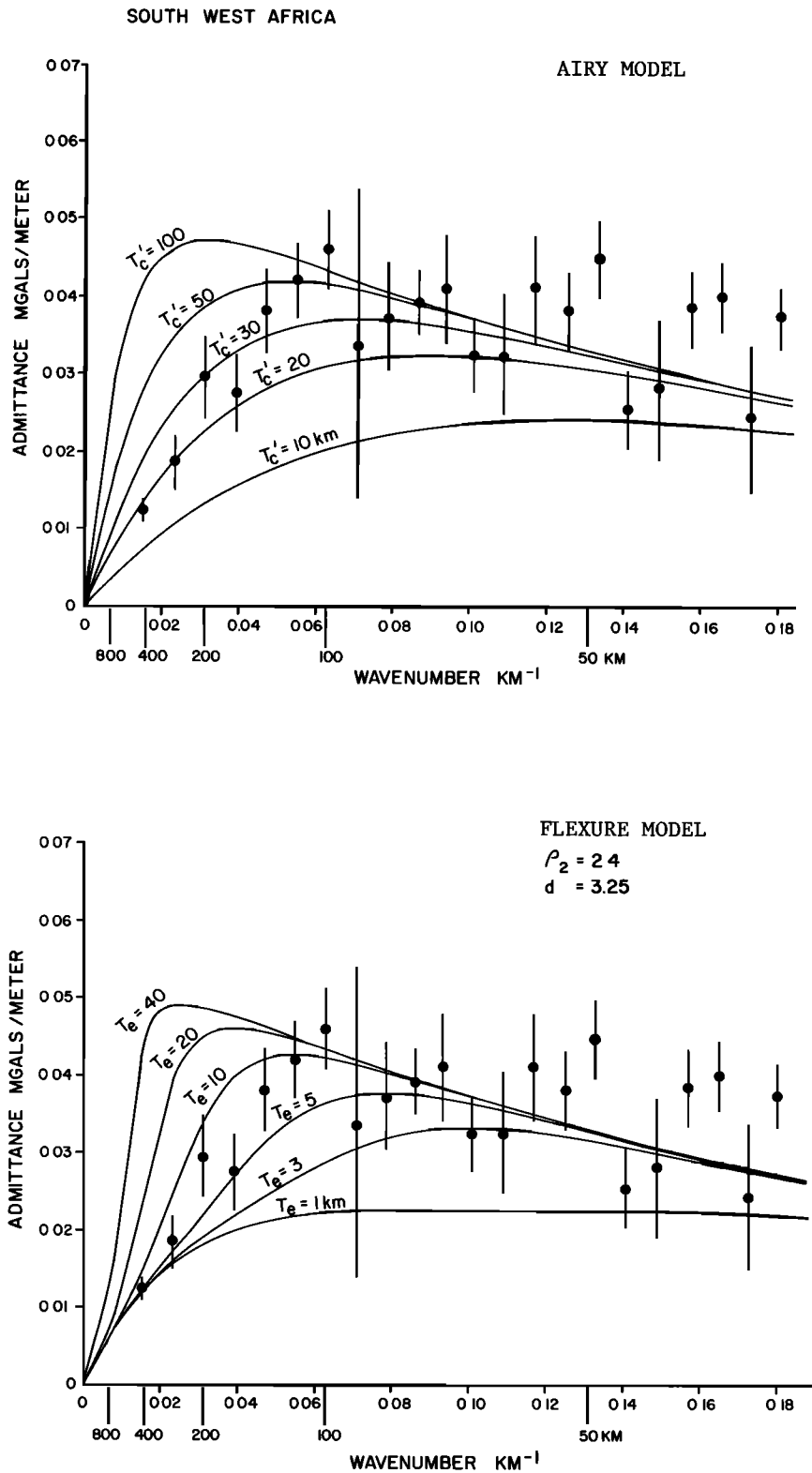


Fig. 7. Observed admittance values (solid circles) for southwest Africa compared with theoretical admittance based on the Airy and flexure models of isostasy.

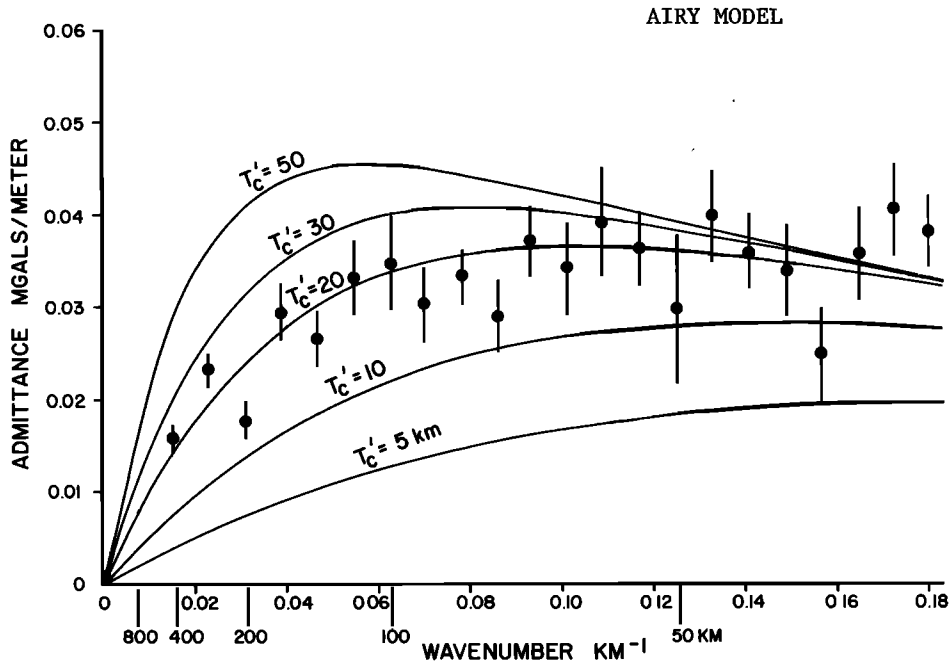
ripping event and the subsequent cooling of the lithosphere with time.

A useful parameter which characterizes the form of lithospheric heating during rifting as well as the crustal structure of the margin is β , the 'lithospheric stretching' factor of McKenzie [1978]. Following Karner and Haxby [1982], if we

assume that the lithospheric dissipation of heat can be approximated by an error function, the density anomaly caused by a general beta distribution $\beta(x)$ is,

$$\Delta\rho(x, z, t) = \alpha\rho_m T_m X(x, t) * \operatorname{erfc} \left\{ \frac{z}{2[\kappa(t + \tau_s)]^{1/2}} \right\} \quad (14)$$

CORAL SEA and LORD HOWE RISE



FLEXURE MODEL

$$\rho_2 = 2.4$$

$$d = 3.0$$

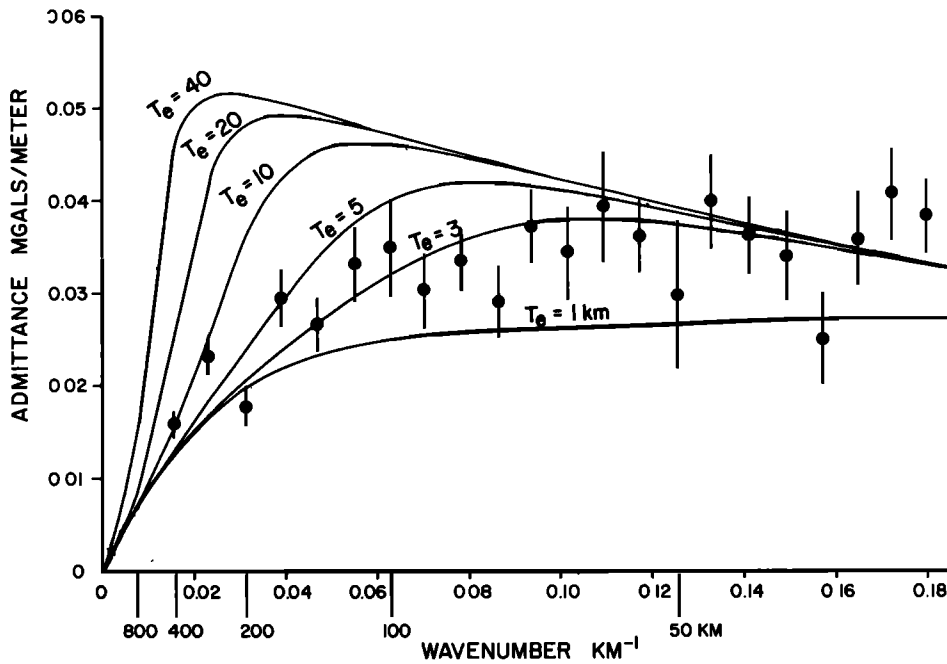


Fig. 8. Observed admittance values (solid circles) for the Coral Sea/Lord Howe rise compared with theoretical admittance models based on the Airy and flexure models of isostasy.

where ρ_m is the lithospheric density at temperature T_m , κ is the thermal diffusivity, t is the time since rifting, $X(x, t)$ is the Green's function for a unit instantaneous plane source and represents the horizontal temperature distribution [Carslaw and Jaeger, 1959], and $*$ is the convolution operation. The

beta distribution is characterized by τ_s , where

$$\tau_s = \tau_0/\beta(x)^2 \tag{15}$$

τ_0 is a calibration constant which defines the transition to nonlinear behavior in the elevation versus (age)^{1/2} curve for

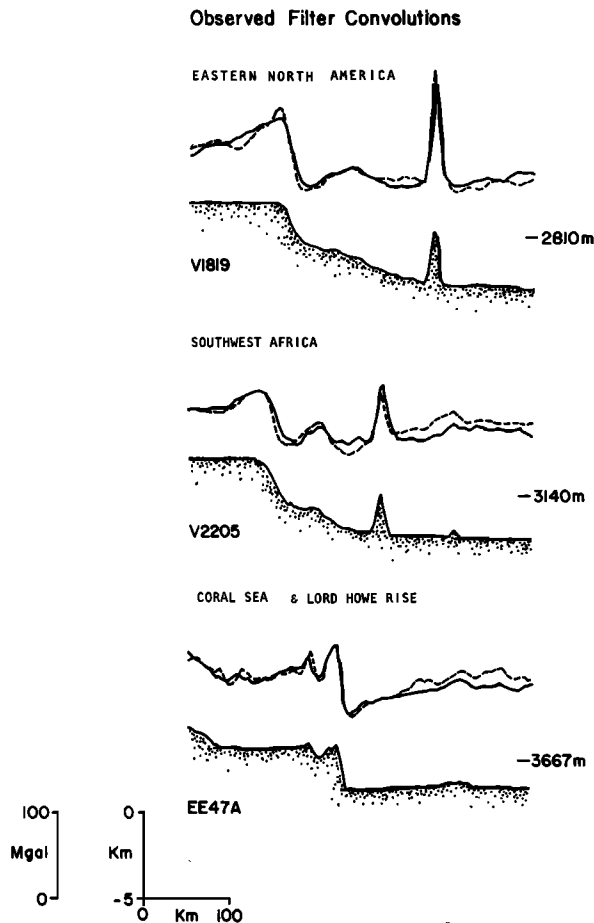


Fig. 9. Observed topography, observed free air gravity anomaly (dashed line) and predicted gravity (solid line) for three selected profiles from each of the margins studied. The predicted gravity anomaly is calculated by filtering the observed topography using the respective observed admittance function for that margin. The similarity between the observed and predicted gravity is indicative of the admittance function's ability to characterize the margin it was constructed from. Cruise identification, mean topographic level, and RMS value indicating the quality of the filtering are given on the left or right of each profile, respectively.

oceanic lithosphere (the C_2 factor of *Parsons and Sclater* [1977]). The various model parameters used in this study are defined in Table 1.

For computational simplicity we first calculate the geoid effect in the frequency domain, and then, by using the inverse Fourier transform, we determine the gravity effect of the anomalous density distribution. By assuming a local

TABLE 1. Model Parameters

Parameter	Value
Water density	$\rho_w = 1.03 \text{ gm/cm}^3$
Sediment density	$\rho_s = 2.5$
Crustal density	$\rho_c = 2.8$
Mantle density	$\rho_m = 3.4$
Young's modulus	$E = 10^{12} \text{ dyn cm}^{-2}$
Poisson's ratio	$\sigma = 0.25$
Thermal conductivity	$\alpha = 3.4 \times 10^{-5} \text{ }^\circ\text{C}^{-1}$
Thermal diffusivity	$\kappa = 8.0 \times 10^{-3} \text{ cm}^2 \text{ s}^{-1}$
Defining lithospheric isotherm	$T_m = 1333 \text{ }^\circ\text{C}$
Calibration coefficient	$\tau_0 = 66 \text{ m.y.}$
Gravitational acceleration	$g = 980 \text{ cm s}^{-2}$

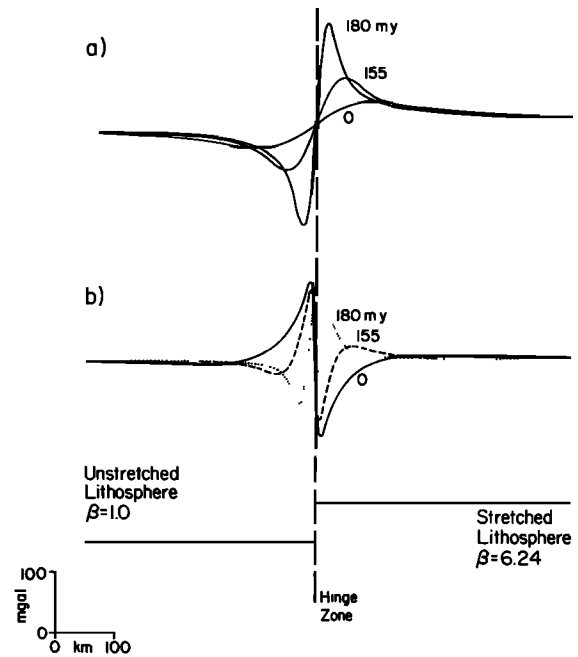


Fig. 10. Theoretical gravity effects over an evolving, sediment starved, Atlantic-type continental margin with time considering thermal isostasy. (a) The gravity effect caused by temperature variations within the lithosphere associated with rifting has been plotted at 0, 25, and 180 m.y. after rifting. The time variation of the gravity effect is a result of horizontal and vertical heatflow through the lithosphere assuming a constant thermal conductivity. The initial input heat distribution is defined by β . (b) The total gravity effect including the crustal structure defined by β is plotted. Airy compensation with $T_c = 32 \text{ km}$ has been assumed for crustal isostasy. By using a step function form for β , the calculated gravity effect across the hinge zone is a maximum.

dipole moment for the density-depth distribution, the geoid effect in the wave domain is given by [*Haxby and Turcotte*, 1978]

$$N(k) = \frac{-2\pi\gamma}{g} \int_0^\infty z \Delta\rho(k, z, t) dz \quad (16)$$

and the gravity effect is [e.g., *Chapman*, 1979]

$$G(k) = -2\pi\gamma k \int_0^\infty z \Delta\rho(k, z, t) dz \quad (17)$$

The maximum gravity effect due to thermal isostasy is given by a β distribution of

$$\begin{aligned} \beta(x) &= 1 & x \leq 0 \\ \beta(x) &= 6.24 & x > 0 \end{aligned} \quad (18)$$

where $\beta = 6.24$ produces a crustal thickness similar to that of oceanic crust. Figure 10a shows the calculated thermal gravity effect associated with $\beta(x)$ and assumes a sediment-starved margin. This thermal gravity effect is similar in overall shape to the margin free air gravity crustal 'edge effect.' The positive gravity peak is now seaward of the hinge zone, however, in marked contrast to the crustal edge effect which has a positive peak landward of the hinge zone (upper model, Figure 5). The two gravity effects compete resulting in a maximum ($\sim \pm 300 \text{ mgal}$) at the time of rifting. With time the total gravity effect rapidly decays in amplitude while increasing in wavelength (Figure 10b). After $\sim 50 \text{ m.y.}$

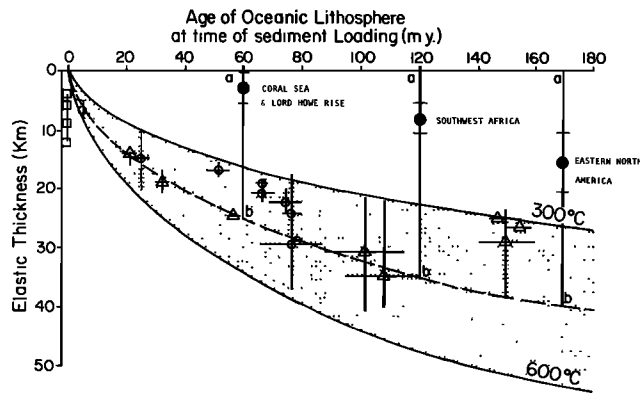


Fig. 11. Plot of effective elastic thickness of the oceanic lithosphere T_e against age of the lithosphere at the time of sediment loading. The sources of data are given by Watts *et al.* [1980]. The open circles and triangles are representative constraints of the variation in T_e from previous studies. The solid lines are the 300°C and 600°C oceanic isotherms based on a cooling plate model. The dotted line represents the approximate mean 450°C isotherm. Superimposed on this plot are the estimates of the effective elastic thicknesses obtained from this study plotted against the age of their respective margins. The range in T_e for a given margin age is indicated by a and b . The a represents sediment loading during the formation of the margin, and so $T_e = 0$. The b represents sediment loading at the margin today. Estimates of T_e at a margin will be constrained by these end members but may plot anywhere between a and b , depending on the loading history.

the thermal anomaly has been essentially reduced to a linear trend across the margin while the crustal effect increasingly dominates the gravity effect. This trend is inversely correlated with the longest topographic wavelength representing the level change from continent to ocean. Therefore the thermal gravity effect is incoherent with all but the longest topographic wavelength and we would not expect it to contribute significantly to the observed admittance functions. However, the thermal effect may be isolated in the isostatic gravity anomaly obtained by convolving theoretical crustal admittances with the margin topography.

We conclude, therefore, that while a significant thermal gravity effect may be present in the gravity anomaly observed at a continental margin, the effect rapidly decays with time becoming essentially a linear trend across the margin. Thus the crustal effect dominates observed gravity anomalies at a margin so that the admittance technique outlined in the previous section can be used to estimate the isostatic parameters that control crustal structure, such as T_e .

DISCUSSION

Studies of the response of the oceanic lithosphere to surface loads, such as oceanic islands and seamounts, show that the effective elastic thickness T_e increases with the age of the lithosphere [for example, Watts *et al.*, 1980]. This suggests that if the lithosphere at a margin has similar mechanical properties as oceanic lithosphere, then sediments loading a margin soon after rifting would be associated with relatively low values of T_e while sediments loading an old margin would be associated with higher values. Seismic and stratigraphic studies of margins [for example, Given, 1977] have shown that sedimentation is initially controlled by fault-bounded crustal blocks (syn- and prerift sediments) and is subsequently replaced by a flexural control (postrift sediments).

Although the mechanical behavior of continental lithosphere is poorly known, T_e would be expected to vary across a margin during its evolution. For example, in the stretching model [McKenzie, 1978], T_e would be relatively small in the region of stretched lithosphere (large β) and relatively large in the region of unstretched continental lithosphere (small β) landward of the hinge zone. Thermal and mechanical modeling of margin subsidence, for which the thermal and mechanical effects are coupled [Steckler, 1981; Steckler and Watts, 1982], suggest that the largest variation in T_e occurs across the hinge zone. Early in margin evolution (<10–20 m.y.), flexure competes with the effects of lateral heat conduction in such a way that the subsidence of the basement seaward of the hinge zone due to sediment loading is similar to that of a low-rigidity (Airy-type) plate. Landward of the hinge zone, however, the effects of lateral heat conduction may result in uplift. Later in margin evolution (>10–20 m.y.), flexure becomes increasingly important, causing subsidence both landward and seaward of the hinge zone. During the first 10–20 m.y. after rifting, therefore, the basement across the hinge zone is effectively decoupled such that its mechanical response is that of a low-rigidity plate. The variation in T_e across the hinge zone only becomes important 10–20 m.y. after rifting because of coupling across the hinge zone. The margin, however, has significantly cooled by this time so that the values of T_e on either side of the hinge zone approach each other. Thus we would expect that the gravity effect caused by variations in T_e would be incoherent with respect to the topography 10–20 m.y. after rifting and hence not represented in the observed admittance functions. The high coherence between gravity and topography at a margin is, in fact, dominated by the shelf break. These considerations suggest that lateral variations in T_e would not be significant and that the estimated T_e satisfactorily represent the average response of the lithosphere to sediment loading in the region of the shelf break.

We compare the results of oceanic plate flexure studies to the results of this study in Figure 11. The point a (Figure 11) indicates the value of T_e which would be expected if all the sediments at each margin were deposited at or soon after rifting. Point b indicates the expected value of T_e if all the sediments formed at the present day. Figure 11 shows that the results of this study (vertical bars) are intermediate in value between a and b ; thus T_e varies during the deposition of the sediments. The actual values of T_e determined from this study are controlled by the average age of the sediment load. The values of T_e closest to a (for example, Coral Sea/Lord Howe rise, southwest Africa) indicate the average age of sediment loading is close to the time of rifting. Values closer to b (for example, eastern North America) indicate an average age of loading later in margin evolution. With continuing sedimentation at margins, therefore, the observed values of T_e approach point b , unless, of course, they are reset by postrifting thermal events.

We point out that the values of T_e obtained in this study only represent the average response of the margin to sediment loads and cannot be used to directly infer information on the tectonic-stratigraphic evolution of margins. A useful approach, however, is to use the values of T_e obtained from oceanic flexure studies, which are based on rapidly emplaced loads (≤ 1.5 m.y.) in order to investigate the development of a margin. Figure 12 shows two simple models in which discrete sediment loads are added to a margin at 30,

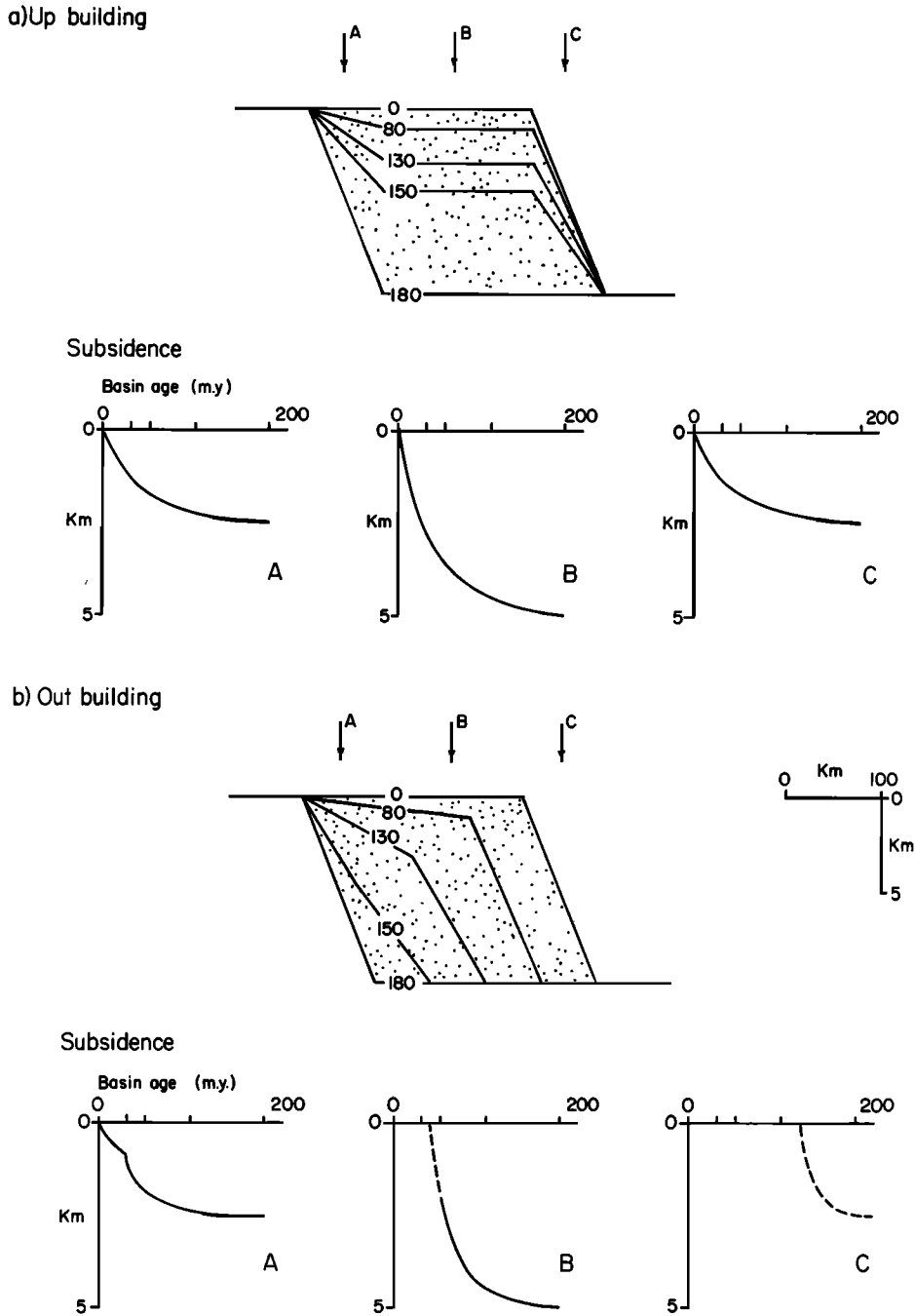
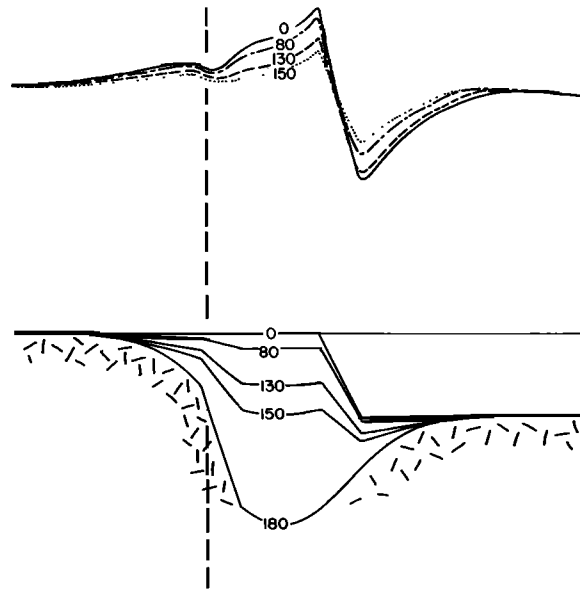


Fig. 12. The development of a sedimentary basin at a continental margin by loading sediment onto an elastic plate in which T_e is increasing with time. For the same tectonic driving force, four loads were placed on the margin at 30, 50, 100, and 180 m.y. after rifting using the two end member mechanisms of basin formation, 'up building,' and 'out building.' (5a) summarizes the theoretical load applied during the development of the margin assuming the sedimentation mode was by up building. (b) summarizes the theoretical load applied during the development of the margin assuming sedimentation was by out building.

50, 100, and 180 m.y. after rifting. The models represent 'end members' of the sedimentary processes by which sediments are supplied to a margin. The lower model represents a prograding margin in which the shelf and slope is maintained by 'out building' whereas the upper model represents a margin which is maintained by 'up building'. For each model we assumed an exponentially decreasing tectonic subsidence (Figure 12) and a T_e which varies during margin evolution according to the dashed curve of Figure 11.

By assuming that continental margins are in isostatic equilibrium during their development and that the flexural strength of the lithosphere increases with time, we are able to predict features of the tectonic-stratigraphic evolution of the margin. Figure 13 shows that the style of basement flexure changes during margin evolution from one of relatively narrow, deep basins to that of broad, shallow basins. These changes in flexural style are associated with overstepping of older strata by younger strata. This is most clearly

a) Up building



b) Out building

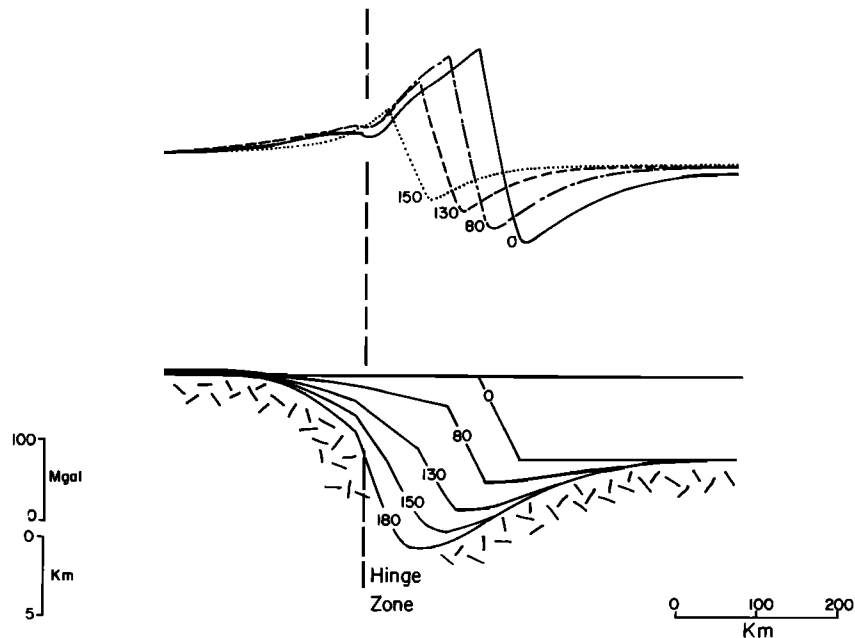


Fig. 13. Theoretical cross sections across continental margins formed by either up building (a) or out building (b) sedimentary processes. The basement response and stratigraphy have been calculated through time using the flexure model and the loading schemes defined in Figure 12. The evolution of the free air gravity anomaly relative to each of the developing margins has also been shown. With time the gravity anomaly reflects the change in isostasy from an initial Airy scheme to increasing uncompensation (for a given profile length) due to sediment loading of a progressively more rigid plate. The different loading schemes predict differences in the margin stratigraphy, basement response, and character of the free air gravity anomaly. Because these loading schemes can be considered as end members of margin development, an actual continental margin may be expected to show examples of both schemes.

seen at the edges of the basin beneath the coastal plain (landward) and continental margin (seaward). The coastal plain, in addition, is associated with uplift during initial loading and subsidence later in loading history.

Figure 13 also shows that the free air gravity anomaly increases in amplitude and wavelength during margin evolution. These changes in the gravity anomaly are a result of the

increasing flexural strength of the lithosphere with time. The gravity anomaly maximum is associated with the load that is added to the margin and follows the shelf edge break, rapidly separating itself from the gravity effect of the hinge zone.

The largest amplitude anomalies occur at the older margins due to continuing sedimentation on a progressively more rigid basement. This result is consistent with Sobczak

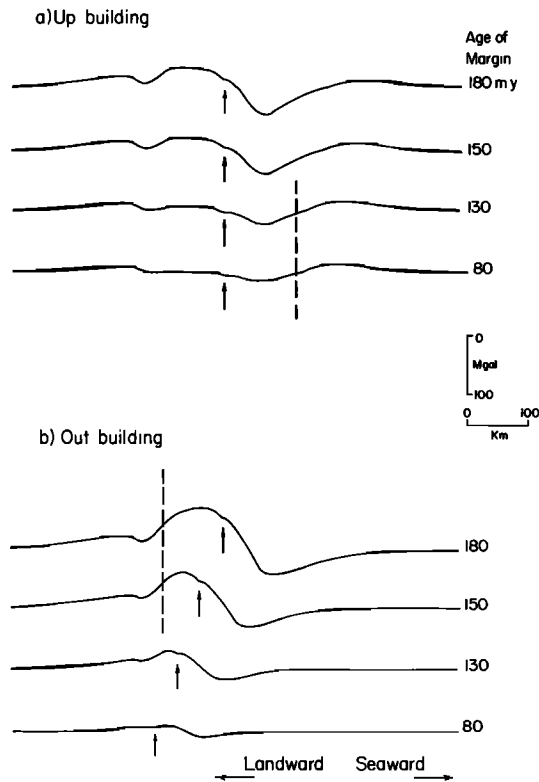


Fig. 14. Isostatic gravity anomalies calculated by applying the 'hidden layer' Airy model to the theoretical topography and free air gravity anomalies of Figure 13. The Airy model assumes two dimensionality, density contrasts of -1.57 and 0.47 gm cm^{-3} at the water-crust and crust-mantle interfaces, respectively, and a depth of compensation $T_c = 32 \text{ km}$. In the up building model (a) the shelf edge (arrowed) is constant, while in the outbuilding model (b) the shelf edge migrates seaward. In either model a steep gradient (dashed line) bounded by a positive anomaly evolves with the margin.

[1975], who pointed out that in order to model the gravity anomaly off Canada, the Tertiary and Recent sediments had to be essentially uncompensated.

The relative importance of flexure to the gravity anomaly through time can be determined by calculating an isostatic anomaly based on Airy isostasy. Figure 14 shows the isostatic gravity anomaly for each of the free air anomaly profiles in Figure 13. The isostatic anomalies are characterized by large-amplitude (up to $\pm 50 \text{ mgal}$) highs and lows separated by a steep gradient (up to 1 mgal/km). The largest amplitude anomalies occur for the older margin (180 m.y.) and the smallest amplitude occur for the younger margin (30 m.y.). Similar amplitude and wavelength isostatic anomalies have been observed for southwest Africa, South Argentina, and eastern North America (Figure 15; see also Rabinowitz [1974], Sobczak [1975], and Rabinowitz and LaBrecque [1979]). It is not possible to directly compare the model results in Figure 14 to any particular margin because its detailed loading history is required. However, comparison of Figures 14 and 15 indicate that the general character of the observed and model isostatic anomalies are very similar.

The isostatic anomalies based on thermal isostasy are, however, in the same sense as the isostatic anomalies due to flexural (crustal) isostasy. Thus thermal and flexural effects, rather than density differences associated with basement highs or the position of the ocean/continent boundary, may

be the main contributors to isostatic gravity anomalies observed at margins.

Figure 16 shows that a number of the features produced by the simple models in Figure 13 can be distinguished at the relatively old eastern North America margin, in particular the broadening of the sediment depocentre with time, the onlapping of relatively young coastal plain sediments (Cretaceous-Tertiary) on older sediments (Jurassic) and continental basement, and the occurrence of both landward and seaward subcrops. Furthermore, although observed free air gravity anomalies reflect in part local density variations, Figure 16 shows the peak gravity anomaly is controlled by the shelf edge and is flanked by a long-wavelength gravity low seaward of the shelf edge and a short-wavelength (or absent) low landward of the shelf edge.

SUMMARY AND CONCLUSIONS

We can make the following summary and conclusions from this study of isostasy at Atlantic-type continental margins.

1. Cross-spectral techniques have been used to analyze the relationship between free air gravity and topography at Atlantic-type continental margins. Three margins were selected based on their age of formation and total sediment thickness. The resulting admittance function contains information common to each margin and has been interpreted in terms of the flexure model of isostasy.

2. The relatively old eastern North America is associated with the highest value of the effective elastic thickness T_e in the range 10–20 km, while the relatively young Coral Sea/Lord Howe rise is associated with the lowest value of T_e of less than 5 km.

3. These estimates of T_e are significantly smaller than those deduced from surface loads on old parts of oceanic

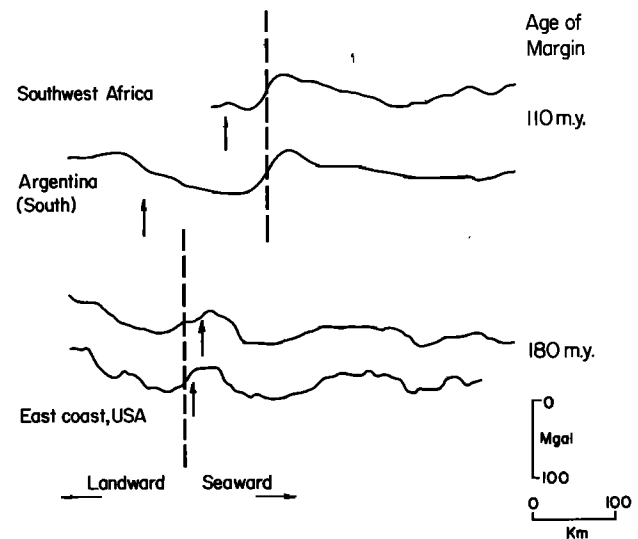


Fig. 15. Airy isostatic gravity anomalies calculated for eastern North America [after Rabinowitz, 1974], southwest Africa and Argentina [after Rabinowitz and LaBrecque, 1979] continental margins. The position of the shelf break and the steep isostatic gravity gradient, interpreted by Rabinowitz and LaBrecque [1977] as representing the position of the ocean-continent boundary, is shown by the arrow and dashed line, respectively. The model isostatic anomalies from Figure 14, for a corresponding aged margin, show a form similar to the observed anomalies, suggesting that flexure, rather than the position of the ocean/continent boundary, may be the main contributor to isostatic gravity anomalies at continental margins.

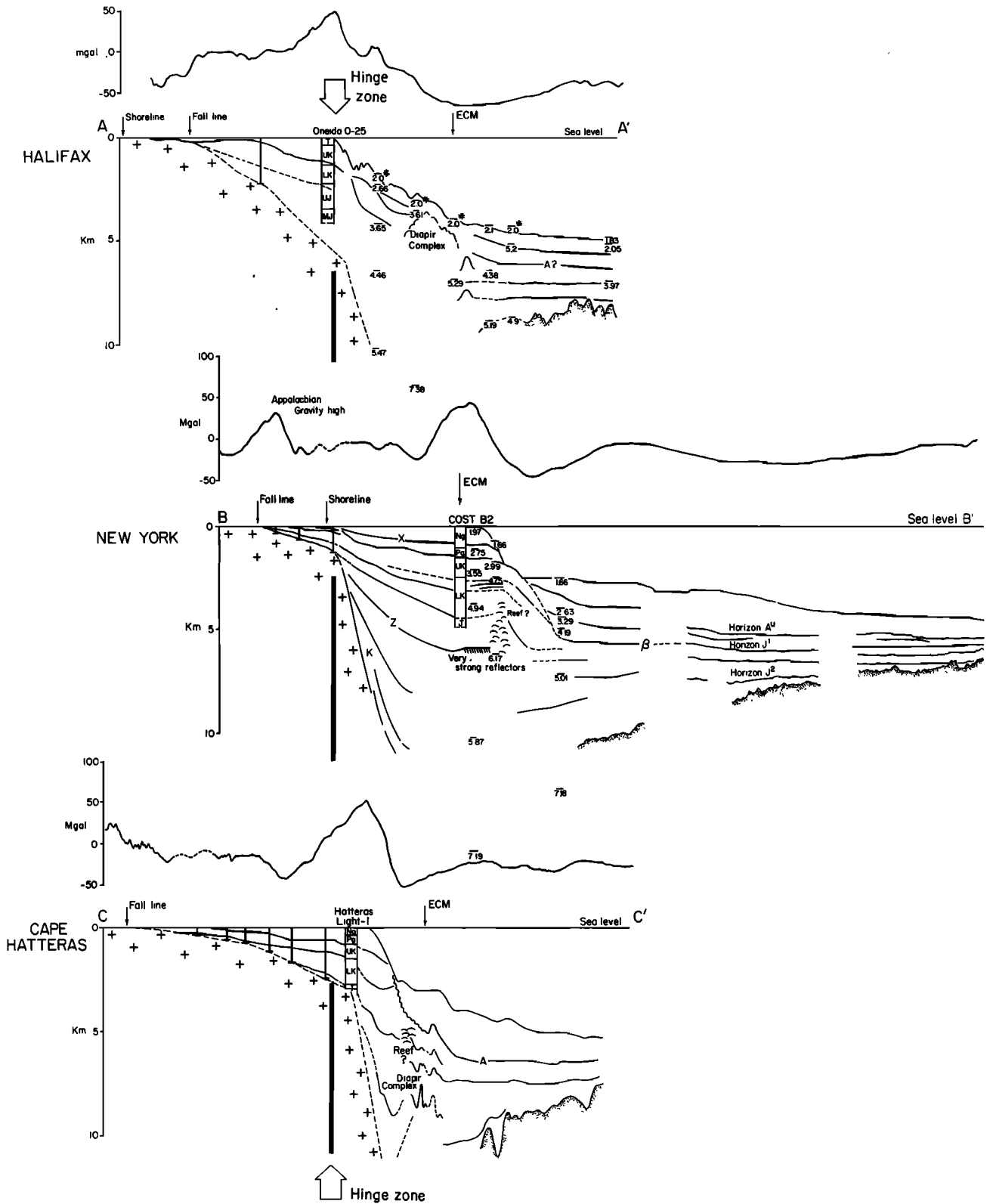


Fig. 16. Summary geologic cross section along the continental margin off North America aligned along the hinge zone (bold line). The stratigraphy of the land boreholes are from Brown et al. [1972]. The stratigraphy of the wells offshore from Nova Scotia are from Williams [1975] and the COST B-2 well from Scholle [1977]. Stratigraphy seaward of the COST B-2 well is from Watts and Steckler [1979] and G. Mountain (personal communication, 1980). The solid lines in the four sections indicate prominent seismic reflectors identified on nearby multichannel seismic profiles [Given, 1977; Grow et al., 1979; Buffler et al., 1979; Dillon et al., 1979]. The arrow labelled ECM refers to the position of the East Coast Magnetic Anomaly. Available refraction seismic velocities [Keen and Loncarevic, 1966; Sheridan et al., 1979] and free air gravity anomalies have also been plotted.

lithosphere (>80 m.y.) but are similar to estimates obtained from admittance studies of the midoceanic ridge crests. This similarity can be explained, since the lithosphere at Atlantic-type continental margins is extensively heated at the time of rifting.

4. The differences in estimates of T_e between margins can be explained by a simple model in which the flexural strength of the basement increases with age. This result is in agreement with studies of isostasy in the world's ocean basins, in which T_e increases with age of the plate at the time of loading.

5. This model explains features of the tectonic-stratigraphic evolution of margins. These include the change in style of basement flexure from narrow to broad basins, the presence of subcrops in which younger sediments overstep older sediments, and the occurrence of an uplifted region in the continental interior which migrates landward with time.

6. Model studies in which different sediment loads are considered suggest that the free air gravity anomaly at a margin changes in both amplitude and wavelength with geological time. The gravity anomaly is determined by the amount and age of the sediments that are supplied and the thermal and mechanical evolution of the margin.

APPENDIX: SPECTRAL ESTIMATES AT ATLANTIC-TYPE CONTINENTAL MARGINS

Analytic Margin Function Spectrum

The use of a limited data window when Fourier transforming a data series precludes a 'true' estimation of the frequency spectrum. The calculated spectrum represents a smoothed, weighted average of the true spectrum. The degree of smoothing depends on the data sample length and the window type used to 'prepare' the signal for transforming. Windows tend to produce side lobe contamination or spectral leakage, and this effect cannot be eliminated. To estimate the degree of contamination in obtaining a spectrum using the discrete, fast Fourier transform, it is necessary to analytically define the topographic and gravimetric transforms of an idealized continental margin.

The topographic spectrum can be theoretically derived by considering a margin as a signum function convolved with a narrow, rectangular gate. The width of the gate determines the continental shelf slope of the margin. It can be shown that the Fourier transform of this function is

$$H(k) = \frac{2i \sin(kT)}{k^2 T} \quad (\text{A1})$$

where $2T$ represents the gate width and k is the wavenumber ($k = 2\pi/\lambda$, where λ is the topographic wavelength). It should be noted that the topographic transform is imaginary. The power spectrum of this same topographic waveform is

$$|H(k)|^2 = \frac{4 \sin^2(kT)}{k^4 T^2} \quad (\text{A2})$$

The general character of the topographic spectra will be controlled by a k^{-4} term with superimposed nodes at values of $k = (2n\pi/T)$, n being an integer. This implies that there are certain frequencies or 'holes' for which there is no topographic energy. As gravity can be considered as upward continued topography, nodes should also appear in the gravity spectrum.

Parker [1973] derived the frequency domain relationship between a topographic surface and the associated free air gravity effect, namely,

$$G(k) = 2\pi\gamma\Delta\rho_1 e^{-kd} \sum_{n=1}^{\infty} \frac{k^{n-1}}{n!} F[h^n(x)] \quad (\text{A3})$$

The topographic surface $h(x)$ is the vertical departure of an interface at any point from its mean depth d and $\Delta\rho_1$ is the density contrast across the interface. For the assumed topographic waveform, it can be shown that

$$F[h^n(x)] = \frac{2}{k} \sum_{l=1}^n \frac{n!}{(n-l)!} \left(\frac{-i}{kT}\right)^l \begin{cases} \sin(kT); & (n-l) \text{ even} \\ i \cos(kT); & (n-l) \text{ odd} \end{cases} \quad (\text{A4})$$

Assuming that this topographic feature is compensated in an Airy-type fashion, the gravimetric transform becomes

$$G(k) = 2\pi\gamma\Delta\rho_1 e^{-kd} \sum_{n=1}^{\infty} \frac{k^{n-1}}{n!} F[h^n(x)] \left(1 - \left[\frac{\Delta\rho_1}{\Delta\rho_2}\right]^{n-1} e^{-kt}\right) \quad (\text{A5})$$

where $\Delta\rho_2$ is the density contrast across the root topography interface which is at mean depth $(d+t)$. Substituting for $F[h^n(x)]$,

$$G(k) = 4\pi\gamma\Delta\rho_1 e^{-kd} \sum_{n=1}^{\infty} \frac{k^{n-2}}{n!} \left[\sum_{l=1}^n \frac{n!}{(n-l)!} \left(\frac{-i}{kT}\right)^l \begin{cases} \sin(kT); & (n-l) \text{ even} \\ i \cos(kT); & (n-l) \text{ odd} \end{cases} \right] \left(1 - \left[\frac{\Delta\rho_1}{\Delta\rho_2}\right]^{n-1} e^{-kt}\right) \quad (\text{A6})$$

The admittance function is defined as the ratio of the gravimetric and topographic transforms. Implicit in the definition of the theoretical linear admittance function (a smoothly varying function) is the existence of 'antinodes' in the gravimetric transform to cancel the topographic nodes. By (A6) the nodes of $G(k)$ rapidly become out of phase with $H(k)$. Necessarily, therefore, the ratio of the gravimetric and topographic transforms will be spiky. The equivalent linear and hence real admittance function of the above topography is simply [McKenzie and Bowin, 1976]

$$Z(k) = 2\pi\gamma\Delta\rho_1 e^{-kd} [1 - e^{-kt}] \quad (\text{A7})$$

Figure A1 compares and contrasts the linear admittance function (A7) with the real part of the complex admittance function calculated from $H(k)$ and $G(k)$ for the first four terms in (A6). Since $H(k)$ is imaginary, the real part of the complex admittance is obtained by the division of the imaginary parts of $G(k)$ and $H(k)$, respectively. Densities and water depths for the eastern North American margin were used to construct the curves, and $2T$, the average width of the continental shelf slope, was set to 100 km. From the comparison of Figure A1 with Figure 6 it would appear that the major spikes in the observed admittance are related to higher order effects of the observed gravity. Being spikes (like transients), they have little energy and so the linear admittance, which satisfactorily explains a large percentage of the observed energy (e.g., Figure 9), can accurately predict the spatial gravity. When interpreting the observed admittance relative to a linear admittance model (for example, Figures 6, 7, and 8), these spikes should be ignored. The

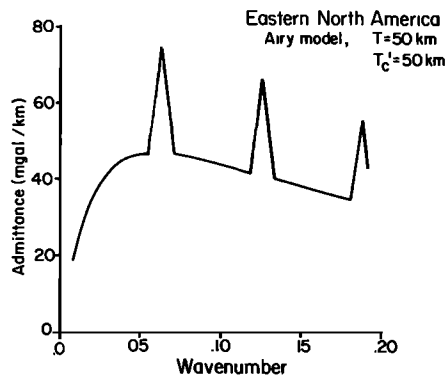


Fig. A1. Theoretical, nonlinear Airy admittance function calculated using (A1) and (A6) with $n = 4$. Values for d , t , and $\Delta\rho_1$ were taken from the eastern North American admittance results. By comparison with the observed admittance function from Figure 6, its spiky nature appears to be related to the nonlinear gravity contribution to the admittance.

spacing of the low-wavenumber spikes can be used to estimate the average width of the shelf slope for the margin studied. Referring to Figure 6 for the eastern North American margin, the spike spacing predicts an average shelf slope width of ~ 74 km.

If the spectra and hence the admittances are averaged for a number of profiles across a margin with varying continental slope (and hence T), the resultant should tend to the linear admittance function. Comparison of the observed with the linear admittance is therefore justifiable.

Systematic Error Analysis

Intrinsic noise is always produced when the Fourier transform is numerically evaluated. The source of this noise is a complicated interaction between various errors associated with windowing, interpolation, and discrete sample lengths. A simple way to investigate this intrinsic noise is to calculate the various spectral estimates for perfect gravity and topography data. To achieve this, free air gravity was numerically calculated over a simple margin shape using the line-integral technique of *Talwani* [1973] and with a known isostatic model.

For this perfect data, the power, coherence, and admittance functions were estimated. As with actual data, this perfect information was linearly interpolated, reflected, and sampled with a rectangular window before transforming.

The complex admittance is obtained by normalizing the gravity transform by the topographic transform. To stabilize the transforms and hence the admittance, it is necessary to perform some type of spectral smoothing. For this study, independent estimates of the topography/gravity relationship were ensembled averaged in the frequency domain to enhance the signal to noise ratio [Parker, 1974].

The gravity and topographic spectra were estimated by using the Fast Fourier Transform (FFT) [Cooley and Tukey, 1965]. Comparison of spectra estimates using both the FFT and the maximum entropy method [Burg, 1968] gave essentially the same averaged spectra verifying the applicability of the FFT. The complex admittance was estimated from the ensembled averaged topographic and gravimetric spectra such that

$$Z(k) = \frac{1}{N} \frac{\sum[G(k) \bar{H}(k)]}{\sum[H(k) \bar{H}(k)]} \quad (\text{A8})$$

where

$$G(k) = G_f(k) * W_f(k) \quad H(k) = H_f(k) * W_f(k)$$

$G_f(k)$ and $H_f(k)$ are the theoretical Fourier transforms of the gravity and topography, respectively, and will always be distorted by the effects of the sampling window, $W(k)$. $G(k)$ and $H(k)$, therefore, are the discrete FFT of gravity and topography, respectively, $\bar{H}(k)$ represents the complex conjugate of $H(k)$, $*$ represents the convolution operation, and N is the number of independent estimates of the admittance, here the number of profiles. Note that the convoluted effects of the window cannot be isolated from the admittance estimates.

Coherence is a measure of that portion of the free air gravity anomaly directly related to the topography and is analogous to the correlation coefficient of regression analysis. Low coherence for low wavenumbers suggests that some isostatic scheme is operative though the decay rate is controlled by the type of compensation; for example, regional isostasy should have a slower decay rate than local compensation. However, the transform of the reflected data is necessarily real, and hence the coherence will remain at unity until imaginary components are produced as the signal to noise ratio decreases. The slope of the ensembled average coherence is therefore an estimate of the severity of the intrinsic noise.

Figure A2 summarizes the spectral estimates obtained when topographic profiles with progressively increasing continental slope and associated free air anomaly (assuming Airy isostasy) were analyzed by the cross-spectral technique. The left column displays the spectral estimates for one profile, while the right column displays the spectral estimates for 10 ensembled averaged profiles.

The main conclusion from this figure is that ensemble averaging is a viable technique for stabilizing the power spectra and admittance. Interpretation of the averaged admittance suggested an Airy model with depth of compensation $T_c = 30$ km, and surface density 2.7 gm cm^{-3} , which is in total agreement with the parameters used to calculate the free air anomaly. However, the predicted average water depth of 1.5 km was underestimated compared to the actual 2.5 km. The dashed lines bounding the admittance represent slopes of 1.04 and 2.02 km. The main purpose for calculating ρ_2 and d is to calibrate the observed and theoretical admittances so that a comparison can be made.

Predictions from the first section of this appendix appear to be validated; in particular, topographic spectral nodes and a very unstable, spiky, admittance function. The high-frequency signal which has been modulated by the type of functions discussed above represents the intrinsic noise introduced by this technique.

Observed Spectral Parameters

Figure A3 summarizes the spectral estimates obtained in this study of isostasy of the eastern North America, southwest Africa, and the Coral Sea/Lord Howe rise margins. All topographic and gravimetric data from these margins were prepared for transforming by linearly interpolating the data to regular spacings, reflecting, removal of the mean from each profile, and finally, truncating the profile to a constant length using a rectangular window.

The resultant ensembled averaged spectra were used to

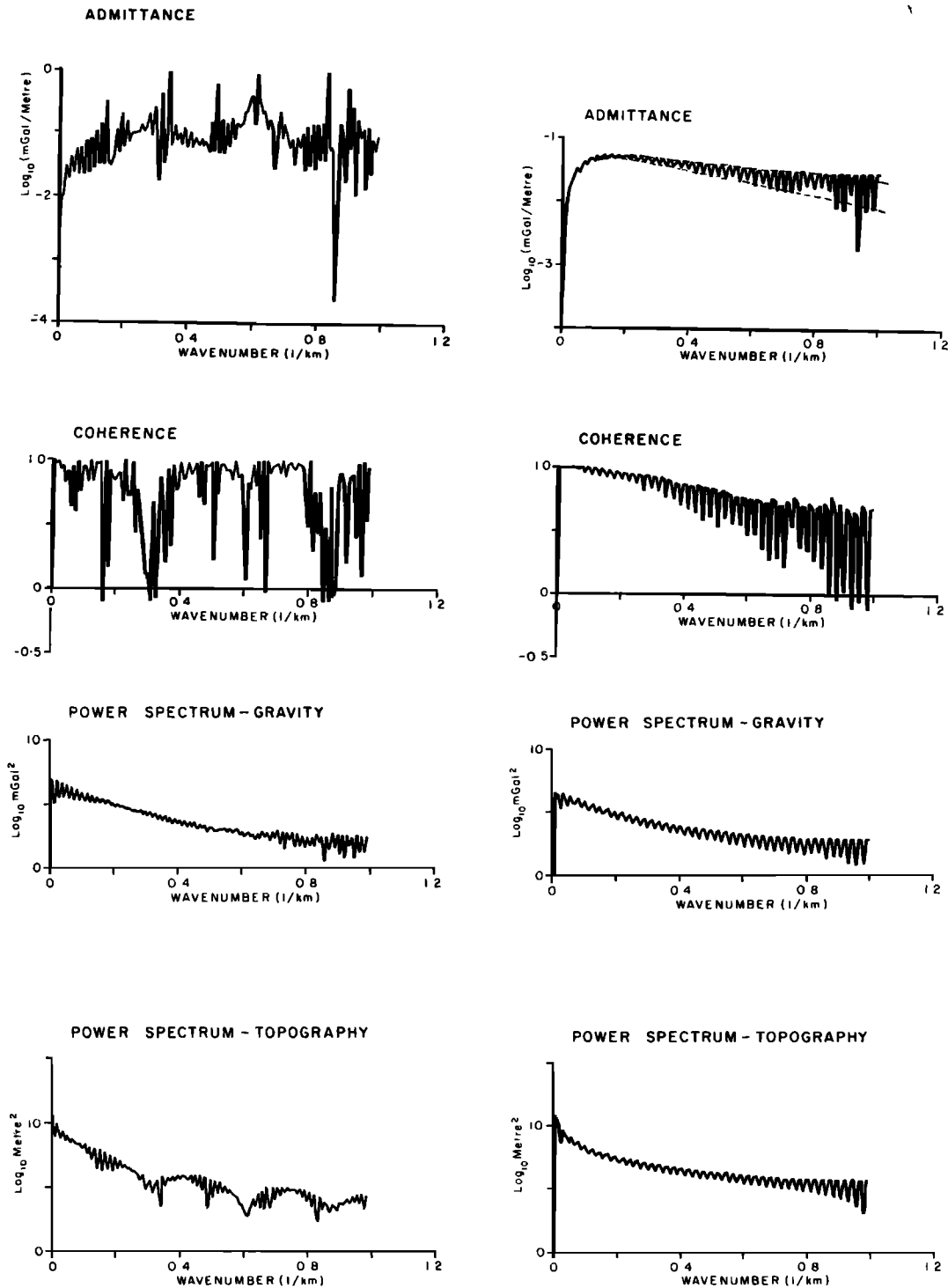
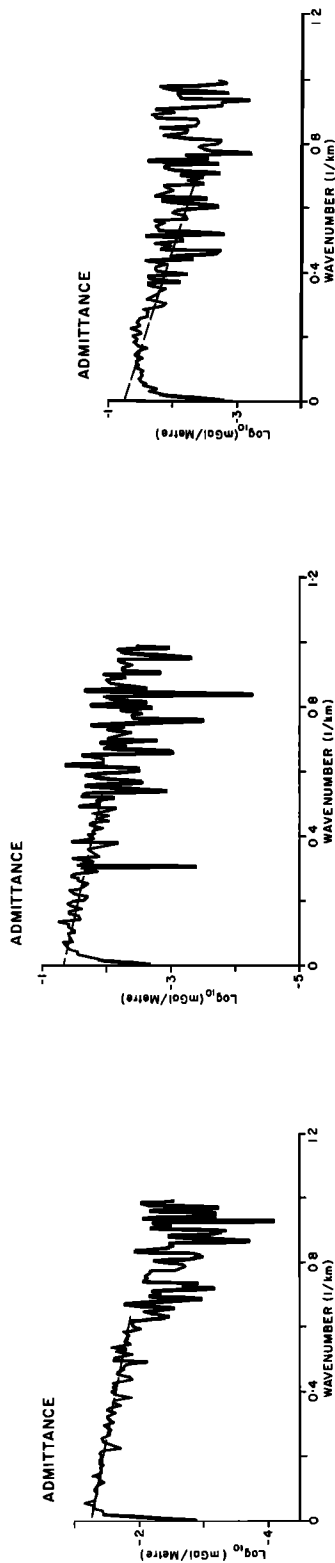
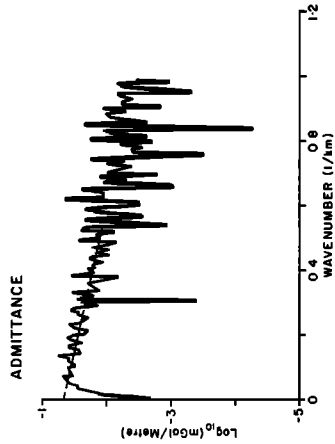
SPECTRAL ESTIMATES
(SINGLE MODEL)SPECTRAL ESTIMATES
(MULTIPLE MODELS)

Fig. A2. Spectral estimate for perfect topography and gravity data. The free air gravity profiles were obtained by using an Airy-type compensation scheme. The single-model results refer to the spectral parameters obtained for only one profile, while the multiple models refer to the spectral parameters obtained for an ensembled average of profiles in which the continental margin slope was varied. Interpretation of the multiple model admittance function returned the input isostatic scheme, verifying the applicability of the cross-spectral technique.

EASTERN NORTH AMERICA



SOUTHWEST AFRICA



CORAL SEA & LORD HOWE RISE

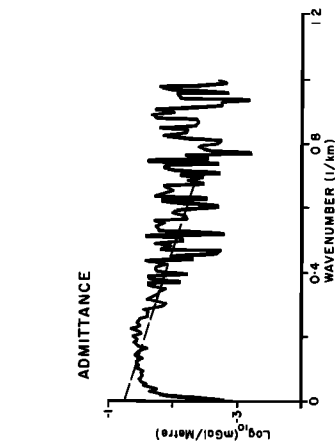


Fig. A3. Summary of spectral estimates for the three margins studied: eastern North America, southwest Africa, and the Coral Sea/Lord Howe rise. The dashed line superimposed on each admittance function represents the regression curve used to estimate P_2 and d for each margin where the respective spectra were nonwhite. Figures 6, 7, and 8 are expanded linear plots of the admittance estimates for $k = 0.0-0.18 \text{ km}^{-1}$.

estimate an admittance function for each of the margins. A least squares linear fit to the data for $k > 0.04$ is shown superimposed on each admittance function and was used to estimate ρ_2 and d for each margin.

Acknowledgments. We wish to thank J. Bodine, W. Haxby, J. LaBrecque, L. Sykes, and J. Thorne for critically reviewing this manuscript. We thank M. Steckler, J. Bodine, R. Whitworth, P. Wellman, and J. Weissel for stimulating discussions, K. Barrell for help in the theoretical derivation of the power spectra, and an anonymous reviewer for pointing out the potential importance of thermal isostasy. L. Karner and R. Weissel provided assistance in computer programming and data processing. We thank the chief scientists and crews of the R.V. *Vema*, R.V. *Conrad*, U.S.N.S. *Eltanin*, and M.V. *Hamme* who collected the gravity and bathymetry data used in this study. This work was supported by NASA contract NAG 5-98, National Science Foundation contract OCE-79-18917, and an Australian Public Service Postgraduate Scholarship to G. D. Karner.

REFERENCES

- Airy, G. B., On the computation of the effect of the attraction of mountain-masses as disturbing the apparent astronomical latitude of stations of geodetic surveys, *Phil. Trans. R. Soc.*, 145, 101-104, 1855.
- Austin, J. A., E. Uchupi, D. R. Shaugnessy, and R. D. Ballard, Geology of the New England passive margin, *Am. Assoc. Pet. Geol. Bull.*, 64, 501-526, 1980.
- Banks, R. J., R. L. Parker, and S. P. Huestis, Isostatic compensation on a continental scale: Local versus regional mechanisms, *Geophys. J. R. Astron. Soc.*, 51, 431-452, 1977.
- Barrell, J., The strength of the Earth's crust, 8, Physical conditions controlling the nature of lithosphere and asthenosphere, *J. Geol.*, 22, 425-443, 1914.
- Bott, M. H. P., Inverse methods in the interpretation of magnetic and gravity anomalies, *Meth. Comput. Phys.*, 13, 133-162, 1973.
- Brown, P. M., J. A. Miller, and F. M. Swain, Structural and stratigraphic frame work and spatial distribution of permeability of the Atlantic coastal plain, North Carolina to New York, *U.S. Geol. Surv. Prof. Pap.* 796, 1972.
- Buffler, R. T., J. S. Watkins, and W. P. Dillon, Geology of the offshore southeast Georgia embayment, U.S. Atlantic continental margin, based on multichannel seismic reflection profiles, *Mem. Am. Assoc. Pet. Geol.*, 29, 11-26, 1979.
- Burg, J. P., A new analysis technique for time series data, paper presented at Advanced Study Institute on Signal Processing, NATO, Enschede, Netherlands, 1968.
- Carslaw, H. S., and J. C. Jaeger, *Conduction of Heat in Solids*, Oxford University Press, 1959.
- Chapman, M. E., Techniques for interpretation of geoid anomalies, *J. Geophys. Res.*, 84, 3793-3802, 1979.
- Cochran, J. R., Gravity and magnetic investigations in the Guiana basin, western equatorial Atlantic, *Geol. Soc. Am. Bull.*, 84, 3249-3268, 1973.
- Cochran, J. R., Analysis of isostasy in the world's oceans, 2, Midocean ridge crests, *J. Geophys. Res.*, 84, 4713-4729, 1979.
- Cooley, J. W., and J. W. Tukey, An algorithm for the machine computation of complex Fourier Series, *Math. Comput.*, 19, 297-301, 1965.
- de Charpal, O., P. Guennoc, L. Montadert, and D. G. Roberts, Rifting, crustal attenuation and subsidence in the Bay of Biscay, *Nature*, 275, 706-711, 1978.
- Dillon, W. P., C. K. Paull, R. T. Buffler, and J. P. Fail, Structure and development of the southeast Georgia embayment and northern Blake Plateau: Preliminary analysis, *Mem. Am. Assoc. Pet. Geol.*, 29, 27-42, 1979.
- Dorman, L. M., and B. T. R. Lewis, Experimental isostasy, 1, Theory of the determination of the earth's isostatic response to a concentrated load, *J. Geophys. Res.*, 75, 3357-3365, 1970.
- Folger, D. W., W. P. Dillon, J. A. Grow, K. D. Klitgord, and J. S. Schlee, Evolution of the Atlantic continental margin of the United States, in *Deep Drilling Results in the Atlantic Ocean: Continental Margins and Paleoenvironment*, Maurice Ewing Ser., vol. 3, edited by M. Talwani, W. Hay, and W. B. F. Ryan, pp. 87-108, AGU, Washington, D. C., 1979.
- Gerrard, I., and G. C. Smith, The post Palaeozoic succession and structure of the south-western African continental margin, *Am. Assoc. Pet. Geol. Memo.*, in press, 1982.
- Given, M. M., Mesozoic and early Cenozoic geology, *Bull. Can. Pet. Geol.*, 25, 63-91, 1977.
- Gray, F., and A. P. Stacey, Gravity and magnetic interpretation of Porcupine Bank and Porcupine Bight, *Deep Sea Res.*, 17, 467-475, 1970.
- Grow, J. A., R. E. Mattick, and J. S. Schlee, Multichannel seismic depth sections and interval velocities over outer continental shelf and upper slope between Cape Hatteras and Cape Cod, *Mem. Am. Assoc. Pet. Geol.*, 29, 65-83, 1979.
- Gunn, R., A quantitative study of the lithosphere and gravity anomalies along the Atlantic coast, *Franklin Inst. J.*, 237, 139-154, 1944.
- Hanks, T. C., The Kuril Trench-Hokkaido rise system: Large shallow earthquakes and simple models of deformation, *Geophys. J. R. Astron. Soc.*, 23, 173-189, 1971.
- Haxby, W. F., and D. L. Turcotte, On isostatic geoid anomalies, *J. Geophys. Res.*, 83, 5473-5477, 1978.
- Heiskanen, W. A., and F. A. Vening Meinesz, *The Earth and its Gravity Field*, McGraw-Hill, New York, 1958.
- Jansa, L. F., and J. A. Wade, Geology of the continental margin off Nova Scotia and Newfoundland, *Geol. Surv. Can. Pap.* 74-30(2), 51-105, 1975.
- Karner, G. D., and W. F. Haxby, Thermal transients associated with sedimentary basin evolution, *J. Geophys. Res.*, in press, 1982.
- Keen, C. E., and B. D. Loncarevic, Crustal structure on the eastern seaboard of Canada: Studies of the continental margin, *Can. J. Earth Sci.*, 3, 65-76, 1966.
- King, P. B., Tectonic map of North America, G67154, U.S. Geol. Surv., Dep. of Inter., Washington, D. C., 1969.
- König, M., and M. Talwani, A geophysical study of the southern continental margin of Australia: Great Australian Bight and western sections, *Geol. Soc. Am. Bull.*, 88(7), 1000-1014, 1977.
- Larson, R. L., and J. W. Ladd, Evidence for the opening of the south Atlantic in the early cretaceous, *Nature*, 246, 209-212, 1973.
- Lewis, B. T. R., and L. M. Dorman, Experimental isostasy, 2, An isostatic model for the U.S.A. derived from gravity and topography data, *J. Geophys. Res.*, 75, 3367-3386, 1970.
- Maher, J. C., and R. R. Applin, Geologic framework and petroleum potential of Atlantic coastal plain and continental shelf, *U.S. Geol. Surv. Prof. Pap.* 659, 98 pp., 1971.
- Mammerickx, J., S. M. Smith, I. L. Taylor, and T. E. Chase, Topography of the South Pacific, *IMR Tech. Rep.*, Ser. TR 56, Inst. of Mar. Resour., La Jolla, Calif., 1974.
- McKenzie, D. P., Some remarks on the development of sedimentary basins, *Earth Planet. Sci. Lett.*, 40, 25-32, 1978.
- McKenzie, D. P., and C. Bowin, The relationship between bathymetry and gravity in the Atlantic ocean, *J. Geophys. Res.*, 81, 1903-1915, 1976.
- McNutt, M., Compensation of oceanic topograph: An application of the response function technique to the SURVEYOR area, *J. Geophys. Res.*, 84, 7589-7598, 1979.
- McNutt, M., and H. W. Menard, Lithospheric flexure and uplifted atolls, *J. Geophys. Res.*, 83, 1206-1212, 1978.
- Mutter, J. C., and G. D. Karner, The continental margin off northeast Australia, *The Geology and Geophysics of Northeastern Australia*, edited by R. A. Henderson and P. J. Stephenson, pp. 47-69, Geological Society of Australia, Queensland Division, Brisbane, 1980.
- Parker, R. L., The rapid calculation of potential anomalies, *Geophys. J. R. Astron. Soc.*, 31, 447-455, 1973.
- Parker, R. L., Stacking marine magnetic anomalies: A critique, *Geophys. Res. Lett.*, 1(6), 259-260, 1974.
- Parsons, B., and J. G. Sclater, An analysis of the variation of ocean floor bathymetry and heat flow with age, *J. Geophys. Res.*, 82, 803-827, 1977.
- Pratt, J. H., On the attraction of the Himalaya Mountains, and of the elevated regions beyond them, upon the plumb line in India, *Phil. Trans. R. Soc.*, 145, 53-100, 1855.
- Rabinowitz, P. D., The boundary between oceanic and continental crust in the western North Atlantic, in *The Geology of Continen-*

- tal Margins*, edited by C. A. Burke and C. L. Drake, pp. 67–84, 1974.
- Rabinowitz, P. D., Geophysical study of the continental margin of southern Africa, *Geol. Soc. Am. Bull.*, 87, 1643–1653, 1976.
- Rabinowitz, P. D., and J. L. LaBrecque, The isostatic gravity anomaly: Key to the evolution of the ocean-continent boundary at passive continental margins, *Earth Planet. Sci. Lett.*, 35, 145–150, 1977.
- Rabinowitz, P. D., and J. LaBrecque, The Mesozoic South Atlantic ocean and evolution of its continental margins, *J. Geophys. Res.*, 84, 5973–6002, 1979.
- Scholle, P. A., Geological studies of the COST B-2 well, United States Mid-Atlantic outer continental shelf area, *U.S. Geol. Surv. Circ. 750*, 1–3, 1977.
- Schouten, H., and K. D. Klitgord, Map showing mesozoic magnetic anomalies, western northern Atlantic, scale 1 : 2,000,000, *Misc. Field Stud. Map M-F-915*, U.S. Geol. Surv., Dep. of Inter., Washington, D. C., 1977.
- Sheridan, R. E., J. A. Grow, J. C. Behrendt, and K. C. Bayer, Seismic refraction study of the continental edge off the eastern United States, *Tectonophysics*, 59, 1–26, 1979.
- Shipboard Scientific Party, Cape Basin continental rise-sites 360 and 361, *Initial Rep. Deep Sea Drill. Proj.*, 40, 29–75, 1978.
- Sleep, N. H., Thermal effects of the formation of Atlantic continental margins by continental breakup, *Geophys. J. R. Astron. Soc.*, 24, 325–350, 1971.
- Sobczak, L. W., Gravity anomalies and passive continental margins, Canada and Norway, *Mem. Can. Soc. Pet. Geol.*, 4, 743–762, 1975.
- Steckler, M. S., The thermal and mechanical evolution of Atlantic-type continental margins, Ph.D. thesis, Columbia Univ., New York, 1981.
- Steckler, M. S., and A. B. Watts, Subsidence of the Atlantic-type continental margin off New York, *Earth Planet. Sci. Lett.*, 41, 1–13, 1978.
- Steckler, M. S., and A. B. Watts, Subsidence history and tectonic evolution of Atlantic-type continental margins, in *Dynamics of Passive Margins, Geodyn. Ser.*, vol. 6, edited by R. A. Scrutton, pp. 184–196, AGU, Washington, D. C., 1982.
- Talwani, M., Computer usage in the computation of gravity anomalies, *Meth. Comput. Phys.*, 13, 343–389, 1973.
- Talwani, M., and O. Eldholm, Continental margin off Norway: A geophysical study, *Geol. Soc. Am. Bull.*, 83, 3575–3606, 1972.
- Talwani, M., and O. Eldholm, The boundary between continental and oceanic crust at the margin of rifted continents, *Nature*, 241, 325–330, 1973.
- Taylor, L., and D. Falvey, Queensland Plateau and Coral Sea basin: Stratigraphy, structure and tectonics, *APEA J.*, 17, 13–29, 1977.
- Uchupi, E., Bathymetric atlas of the Atlantic, Caribbean and Gulf of Mexico, *WHOI Ref. 71-72*, Woods Hole Oceanogr. Inst., Woods Hole, Mass., 1971.
- Van Hinte, J. E., A Jurassic time scale, *Am. Assoc. Pet. Geol. Bull.*, 60, 489–497, 1976.
- Van Houten, F. B., Triassic-Liassic deposits of Morocco and eastern North America: Comparison, *Am. Assoc. Pet. Geol. Bull.*, 61, 79–99, 1977.
- Vening Meinesz, F. A., Gravity over the Hawaiian Archipelago and over the Madiera area: Conclusions about the Earth's crust, *Proc. K. Ned. Akad. Wet.*, 44, 1–44, 1941.
- Walcott, R. I., Flexural rigidity, thickness, and viscosity of the lithosphere, *J. Geophys. Res.*, 75, 3941–3954, 1970.
- Walcott, R. I., Gravity, flexure and the growth of sedimentary basins at a continental edge, *Geol. Soc. Am. Bull.*, 83, 1845–1848, 1972.
- Watts, A. B., An analysis of isostasy in the world's oceans, 1, Hawaiian-Emperor seamount chain, *J. Geophys. Res.*, 83, 5989–6004, 1978.
- Watts, A. B., and J. R. Cochran, Gravity anomalies and flexure of the lithosphere along the Hawaiian-Emperor seamount chain, *Geophys. J. R. Astron. Soc.*, 38, 119–141, 1974.
- Watts, A. B., and W. B. F. Ryan, Flexure of the lithosphere and continental margin basins, *Tectonophysics*, 36, 25–44, 1976.
- Watts, A. B. and M. S. Steckler, Subsidence and eustasy at the continental margin of eastern North America, in *Deep Drilling Results in the Atlantic Ocean: Continental Margins and Paleoenvironment, Maurice Ewing Ser.*, vol. 3, edited by M. Talwani, W. Hay, and W. B. F. Ryan, pp. 218–234, AGU, Washington, D. C., 1979.
- Watts, A. B., J. H. Bodine, and N. M. Ribe, Observations of flexure and the geological evolution of the Pacific Ocean basin, *Nature*, 283, 532–537, 1980.
- Weissel, J. K., and D. E. Hayes, Evolution of the Tasman Sea reappraised, *Earth Planet. Sci. Lett.*, 36, 77–84, 1977.
- Weissel, J. K., and A. B. Watts, Tectonic evolution of the Coral Sea basin, *J. Geophys. Res.*, 84, 4572–4582, 1979.
- Willcox, J. B., P. A. Symonds, K. Hinz, and D. Bennett, Lord Howe Rise, Tasman Sea—Preliminary geophysical results and petroleum prospects, *BMR J. Aust. Geol. Geophys.*, 5, 225–236, 1980.
- Williams, G. L., Dinoflagellate and spore stratigraphy of the Mesozoic-Cenozoic, offshore eastern Canada, *Geol. Surv. Pap. Geol. Surv. Can.*, 74-30, 107–161, 1975.
- Worzel, J. L., Deep structure of coastal margins and mid-oceanic ridges, *Colston Pap. 17*, 335–361, 1965.

(Received April 3, 1981;
revised December 7, 1981;
accepted December 18, 1981.)